ΕΛΛΗΝΙΚΗ ΔΗΜΟΚΡΑΤΙΑ
ΥΠΟΥΡΓΕΙΟ
ΑΝΑΠΤΥΞΗΣ ΚΑΙ ΕΠΕΝΔΥΣΕΩΝ
ΕΙΔΙΚΗ ΓΡΑΜΜΑΤΕΙΑ ΔΙΑΧΕΙΡΙΣΗΣ
ΠΡΟΓΡΑΜΜΑΤΩΝ ΕΤΠΑ & ΤΣ

ΕΣΠΑ 2014-2020
ανάπτυξη - εργασία - αλληλεγγύη

Με τη συγχρηματοδότηση της Ελλάδας και της Ευρωπαϊκής Ένωσης

Δράση ΕΡΕΥΝΩ – ΔΗΜΙΟΥΡΓΩ – ΚΑΙΝΟΤΟΜΩ

Συγχρηματοδότηση από την Ευρωπαϊκή Ένωση και τους εθνικούς πόρους μέσω του Ε.Π. Ανταγωνιστικότητα, Επιχειρηματικότητα & Καινοτομία (ΕΠΑνΕΚ)

ΡΑΝΤΑΡ

“ Ετερογενής Τρισδιάστατη Ολοκλήρωση με χρήση ρηξικέλευθων νανοτεχνολογιών για τη νέα γενιά μικροκυματικών πομποδεκτών ισχύος ”

Κωδικός έργου° Τ1ΕΔΚ-00329

Ενότητα εργασίας 3: Τεχνολογικά Πρωτόκολλα

Παραδοτέο Π3.6

Τίτλος Παραδοτέου:

Ετήσιες αναφορές για διάχυση αποτελεσμάτων της ΕΕ3

Ημερομηνία : Μ30, Μ54

Επικεφαλής παραδοτέου: ΙΤΕ

Με τη συγχρηματοδότηση της Ελλάδας και της Ευρωπαϊκής Ένωσης

Περιεχόμενα

1. Αντικείμενο της Αναφοράς 2

2. Δραστηριότητες προβολής του έργου και διάχυσης των αποτελεσμάτων του έργου 3

2.1. Δημοσιεύσεις σε διεθνή περιοδικά και συνέδρια (acknowledging RADAR) 3

1. Αντικείμενο της Αναφοράς

Αντικείμενο της παρούσας αναφοράς είναι η καταγραφή των ενεργειών που πραγματοποιήθηκαν καθ' όλη την διάρκεια του έργου για τη διάχυση των αποτελεσμάτων της έρευνας στα πλαίσια της **ΕΕ3- Τεχνολογικά πρωτόκολλα** του έργου ΡΑΝΤΑΡ.

Έχει δημιουργηθεί από την έναρξη του έργου ιστότοπος. Ο ιστότοπος παρουσιάζει τα προφίλ των εταίρων της κοινοπραξίας και τις δράσεις διάχυσης. Η τακτική προώθηση των ειδήσεων και των εκδηλώσεων του έργου γίνεται μέσω αυτού, ο οποίος παραμένει ακόμα ενεργός.

Η κοινοπραξία φρόντισε για όλη την διάρκεια του έργου να δημοσιεύονται τα αποτελέσματα σε περιοδικά και να ανακοινώνονται σε σημαντικά διεθνή συνέδρια.

Οι δραστηριότητες προβολής του έργου και διάχυσης των αποτελεσμάτων του έργου περιλαμβάνουν και συμμετοχή σε εκδηλώσεις "ανοικτής ημέρας", παρουσιάσεις και ομιλίες κατά τη διάρκεια της "Βραδιάς του Ευρωπαίου Ερευνητή" και της "Μάθε περισσότερα, γίνε καλύτερος" εκπαιδευτικές δράσεις αφιερωμένες στα σχολεία. Φυλλάδια και δελτία θα παρουσιάζουν εκλαϊκευμένα τα αποτελέσματα του έργου στο ευρύ κοινό.

ΕΣΠΑ 2014-2020

Με τη συγχρηματοδότηση της Ελλάδας και της Ευρωπαϊκής Ένωσης

2. Δραστηριότητες προβολής του έργου και διάχυσης των αποτελεσμάτων του έργου

2.1. Δημοσιεύσεις σε διεθνή περιοδικά και συνέδρια (acknowledging RADAR)

- D. Birmpiliotis et al., "A comparative study of nanostructured Silicon-Nitride electrical properties for potential application in RF-MEMS capacitive switches", Microelectronics Reliability Volumes 100–101, September 2019, 113360, (**https://doi.org/10.1016/j.microrel.2019.06.052**)

Microelectronics Reliability 100–101 (2019) 113360

Contents lists available at ScienceDirect

Microelectronics Reliability

journal homepage: www.elsevier.com/locate/microrel

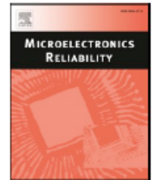

A comparative study of nanostructured Silicon-Nitride electrical properties for potential application in RF-MEMS capacitive switches

D. Birmpiliotis[a,*], G. Stavrinidis[b], M. Koutsoureli[a], G. Konstantinidis[b], G. Papaioannou[a], A. Ziaei[c]

[a] *Physics Department, Solid State Physics Section, University of Athens, Athens 15784, Greece*
[b] *Institute of Electronic Structure and Laser (IESL), Foundation for Research and Technology- Hellas (FORTH), Heraklion 70013, Greece*
[c] *Thales Research and Technology, F-91767 Palaiseau, France*

ABSTRACT

The present paper aims to investigate the electrical properties of nanostructured SiNx with embedded (i) CNTs of random orientation, (ii) columnar bunches of vertically aligned CNTs and (iii) columnar Au nanorods. MIM capacitors were used to assess the effect of dielectric film structure on the electrical properties. The charge transport mechanism was assessed through current - voltage characteristics and the charge draining efficiency through the top electrode potential decay. In the case of random oriented CNTs, the transport mechanisms are Frenkel-Poole and field emission at low and high electric fields respectively. In the case of Au nanorods, the hopping and Frenkel-Poole mechanisms are detected at low and high electric fields respectively. Finally, for vertically aligned CNTs the current-voltage characteristic is found to follow ohm's law. The discharge rate through the bulk material is found to depend on nanofillers morphology.

Acknowledgements

This work is partially co-financed by Greece and the European Union (European Social Fund-ESF) through the Operational Programme «Human Resources Development, Education and Lifelong Learning» in the context of the project "Strengthening Human Resources Research Potential via Doctorate Research" (MIS-5000432), implemented by the State Scholarships Foundation (ΙΚΥ). Also has been co-financed by the European Union and Greek national funds through the Operational Program Competitiveness, Entrepreneurship and Innovation, under the call RESEARCH – CREATE – INNOVATE (Project code: T1EDK-00329).

Με τη συγχρηματοδότηση της Ελλάδας και της Ευρωπαϊκής Ένωσης

- M. Koutsoureli et al., "Thermally activated discharging mechanisms in SiNx films with embedded CNTs for RF MEMS capacitive switches", Microelectronic Engineering Volume 223, 15 February 2020, 111230, (https://doi.org/10.1016/j.mee.2020.111230)

Microelectronic Engineering 223 (2020) 111230

Contents lists available at ScienceDirect

Microelectronic Engineering

journal homepage: www.elsevier.com/locate/mee

Research paper

Thermally activated discharging mechanisms in SiN_x films with embedded CNTs for RF MEMS capacitive switches

M. Koutsoureli[a,*], G. Stavrinidis[b], D. Birmpiliotis[a], G. Konstantinidis[b], G. Papaioannou[a]

[a] *Section of Condensed Matter Physics, National and Kapodistrian University of Athens, Athens 15784, Greece*
[b] *IESL –FORTH, GR-71110 Heraklion, Greece*

ARTICLE INFO

Keywords:
RF MEMS switches
Dielectric charging
Nanostructured dielectrics
Silicon nitride

ABSTRACT

In the present work, we investigate thermally activated processes in nanostructured SiN_x films with embedded CNTs, which can be used in RF MEMS capacitive switches. Nanostructured films have been fabricated with a simple process, in order to incorporate CNTs on the lower SiN_x layer and a reference SiN_x material has been also fabricated with the same method (without CNTs), in order to compare the properties of the nanostructured films with the pristine material. Thermally stimulated depolarization currents (TSDC) assessment and a single-point Kelvin Probe (KP) system have been used in MIM capacitors, in order to investigate the electrical properties of the utilized films.

The nanostructured material is found to exhibit lower charging and smaller discharging time, which makes it a promising candidate for RF MEMS capacitive switches. Thermally activated discharging mechanisms have been identified and the presence of CNTs is found to diminish a discharging mechanism with a characteristic time larger than five days at room temperature. Different discharging mechanisms are identified and distinguished for the first time, to the best of our knowledge, between a reference and a nanostructured SiN_x dielectric film. Charge displacement in the bulk material during discharge takes place through hopping processes and larger mean hopping distance and zero field conductivity has been found in the nanostructured films. The reduction of the discharge characteristic time and the simultaneous suppression of trapping centers in the films with embedded CNTs indicate a direct relation between the macroscopic electrical properties and the microscopic defects in the dielectric material.

Acknowledgements

This work has been financed by the European Union and Greek national funds through the Operational Program Competitiveness, Entrepreneurship and Innovation, under the call RESEARCH – CREATE – INNOVATE. (Project code: T1EDK-00329).

Με τη συγχρηματοδότηση της Ελλάδας και της Ευρωπαϊκής Ένωσης

- S. Birmpiliotis et al., "A study of hopping transport during discharging in SiNx films for MEMS capacitive switches", Microelectronics Reliability Volume 114, November 2020, 113878 (https://doi.org/10.1016/j.microrel.2020.113878)

Microelectronics Reliability 114 (2020) 113878

Contents lists available at ScienceDirect

Microelectronics Reliability

journal homepage: www.elsevier.com/locate/microrel

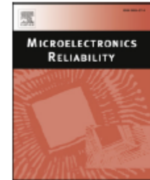

A study of hopping transport during discharging in SiN_x films for MEMS capacitive switches

D. Birmpiliotis[a,*], M. Koutsoureli[a], G. Stavrinidis[b], G. Konstantinidis[b], G. Papaioannou[a]

[a] Condensed Matter Physics Section, University of Athens, GR-15784 Athens, Greece
[b] Institute of Electronic Structures and Lasers (IESL), Foundation for Research and Technology Hellas (FORTH), Heraklion 70013, Greece

ABSTRACT

A more realistic approach of the discharging process in MEMS capacitive switches is presented with the introduction of the effective temperature in order to determine the behavior of the microscopic parameters of hopping conduction, which dominates the process. The use of Kelvin Probe method in MIM capacitors that simulates the discharging process in MEMS switches during up-state revealed that both the increase of temperature and stressing field intensity results the decrease of mean hopping length. This result arises from the simultaneous contribution of the transport energy levels associated with the impact of the stressing field and temperature. Also, a correlation was found experimentally between the stretched exponential decay and the hopping process. The proposed method was also applied in MEMS switches where a similar behavior of the hopping parameters was found, providing evidence that the control of the hopping length to an optimum value can provide fast discharging and low leakage currents, increasing the device lifetime.

Acknowledgements

This work is partially co-financed by Greece and the European Union (European Social Fund-ESF) through the Operational Programme "Human Resources Development, Education and Lifelong Learning" in the context of the project "Strengthening Human Resources Research Potential via Doctorate Research" (MIS-5000432), implemented by the State Scholarships Foundation (IKY). Also has been co-financed by the European Union and Greek National Funds through the Operational Program Competitiveness, Entrepreneurship and Innovation, under the call RESEARCH – CREATE – INNOVATE (Project code: T1EDK-00329).

ΕΣΠΑ 2014-2020
ανάπτυξη - εργασία - αλληλεγγύη

Με τη συγχρηματοδότηση της Ελλάδας και της Ευρωπαϊκής Ένωσης

- J. Theocharis et al., “Impact of dielectric film thickness on field emission in MEMS capacitive switches”, Microelectronics Reliability Volume 138, November 2022, 114649 (https://doi.org/10.1016/j.microrel.2022.114649)

Microelectronics Reliability 138 (2022) 114649

Contents lists available at ScienceDirect

Microelectronics Reliability

journal homepage: www.elsevier.com/locate/microrel

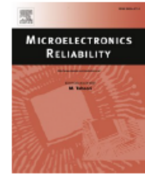

Impact of dielectric film thickness on field emission in MEMS capacitive switches

J. Theocharis *, S. Gardelis, G. Papaioannou

Condensed Matter Physics Section, Physics Department, National and Kapodistrian University of Athens (NKUA), Panepistimiopolis Zografos, 15784 Athens, Greece

ARTICLE INFO

Keywords:
MEMS
Dielectrics
Field emission
Controlled environment
Electrical characterization

ABSTRACT

This study presents experimental evidence of field emission in MEMS capacitive switches. Devices with dielectric layers of silicon nitride of different thicknesses between 50 and 200 nm were investigated by current-voltage (I-V) measurements. These measurements were performed at room temperature and under a controlled atmosphere pressure of 3×10^{-2} mbar at bias levels below breakdown and corresponding electric fields encountered in MEMS capacitive switches during pull-in (1-2 $\times 10^6$ V/cm). Field emission although was not always clearly observed, it occurred in all devices and clearly manifested at electric fields larger than 10^6 V/cm.

Acknowledgements

The present work has been financed by the European Union and Greek national funds through the Operational Program Competitiveness, Entrepreneurship and Innovation, under the call RESEARCH – CREATE – INNOVATE (project code: T1EDK-00329).

Microelectronics Reliability 100–101 (2019) 113360

Contents lists available at ScienceDirect

Microelectronics Reliability

journal homepage: www.elsevier.com/locate/microrel

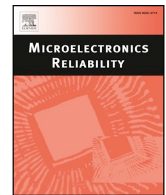

A comparative study of nanostructured Silicon-Nitride electrical properties for potential application in RF-MEMS capacitive switches

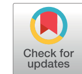

D. Birmpiliotis[a,*], G. Stavrinidis[b], M. Koutsoureli[a], G. Konstantinidis[b], G. Papaioannou[a], A. Ziaei[c]

[a] Physics Department, Solid State Physics Section, University of Athens, Athens 15784, Greece
[b] Institute of Electronic Structure and Laser (IESL), Foundation for Research and Technology- Hellas (FORTH), Heraklion 70013, Greece
[c] Thales Research and Technology, F-91767 Palaiseau, France

ABSTRACT

The present paper aims to investigate the electrical properties of nanostructured SiNx with embedded (i) CNTs of random orientation, (ii) columnar bunches of vertically aligned CNTs and (iii) columnar Au nanorods. MIM capacitors were used to assess the effect of dielectric film structure on the electrical properties. The charge transport mechanism was assessed through current - voltage characteristics and the charge draining efficiency through the top electrode potential decay. In the case of random oriented CNTs, the transport mechanisms are Frenkel-Poole and field emission at low and high electric fields respectively. In the case of Au nanorods, the hopping and Frenkel-Poole mechanisms are detected at low and high electric fields respectively. Finally, for vertically aligned CNTs the current-voltage characteristic is found to follow ohm's law. The discharge rate through the bulk material is found to depend on nanofillers morphology.

1. Introduction

RF-MEMS capacitive switches are promising devices for several applications, especially in the field of wireless communications. Their ultra-high linearity, almost zero power consumption, compatibility with silicon technology and the ability to manage signals close to hundreds GHz, make them the most prominent candidate to succeed the conventional semiconductor based switches [1]. In contrary of these attractive benefits, there are reliability issues, among them the most severe is dielectric charging, hindering their commercialization as "component off-the-shelf". During the devices' operation, specifically during actuation, charges are injected and trapped inside the dielectric causing erratic device behavior, which in most cases may lead to stiction and device failure.

In order to mitigate the dielectric charging significant effort has been paid employing various composition SiNx [2–4]. In all cases the dielectric film has been extensively studied aiming to control its electrical properties considering that beyond the percolation threshold, $x_c = 1.0$, the Si–Si bonds fail to form continuous percolation paths across the network [5]. The intensive study of Si-rich material [6–8] led to better understanding of SiNx electrical properties but still did not provide solution to the persisting problem of dielectric charging.

In a MEMS capacitive switch during up-state the stored charge can only be drained through the bottom electrode, so the ability to quickly remove the injected and trapped charge is essential. In order to enhance this process the first devices with nanostructured dielectric film, with carbon nanotubes (CNTs) embedded in the upper part of the SiNx film was presented by C. Bordas et al. in [9] where they demonstrated that the presence of CNTs improves the device reliability. Considering the effect of percolation and the variable length tunneling taking place in nanostructured dielectrics, their impact on charging mitigation has been discussed in [10].

The present paper aims to investigate, for the first time, the electrical properties of nanostructured SiNx that has been fabricated with different techniques, by embedding (i) CNTs with random orientations, (ii) columnar bunches of aligned CNTs and (iii) columnar Au nanorods. In all cases, the dielectric film has the same thickness and the deposition was performed in two steps of equal thickness where the bottom film was nanostructured. Metal-Insulator-Metal (MIM) capacitors and MEMS capacitive switches were used to assess the effect of dielectric film structure on the electrical properties. The charge transport mechanism was assessed through current - voltage characteristics and the charge draining efficiency through the top electrode potential decay.

2. Experimental data

As already mentioned, MIM capacitors with three different nanostructured dielectrics were fabricated in order to assess dependence of the electrical properties on the material structure. The details of nanostructured dielectric films fabrication is presented below:

* Corresponding author.
E-mail address: dimbir@phys.uoa.gr (D. Birmpiliotis).

https://doi.org/10.1016/j.microrel.2019.06.052
Received 15 May 2019; Received in revised form 12 June 2019; Accepted 21 June 2019
Available online 23 September 2019
0026-2714/ © 2019 Elsevier Ltd. All rights reserved.

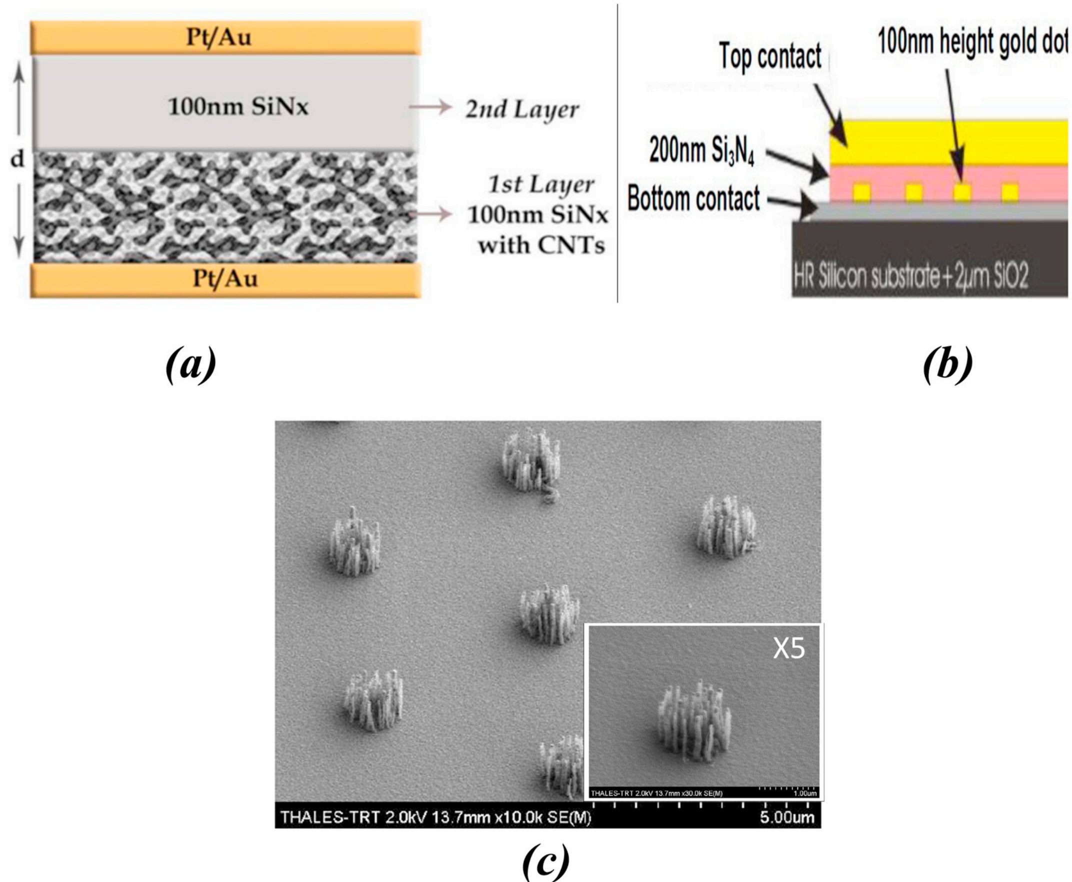

Fig. 1. (a) Schematic of MIM capacitors with randomly oriented CNTs, (b) Schematic of MIM capacitor with Au nanorods, (c) SEM photo of the bunches of vertically aligned CNTs.

2.1. Randomly oriented CNTs

The first group of devices consisted of MIM capacitors with SiNx with embedded CNTs in random orientations (Fig. 1a). The MIM capacitors have symmetrical metal contacts (Au/Pt/dielectric film/Pt/Au) in order to avoid insulator-contacts work function differences and contact area of 1 mm diameter. The dielectric film total thickness was 200 nm SiNx with embedded CNTs in the lower 100 nm film, detailed description presented in [11].

2.2. Vertically aligned CNTs

The devices of this group were fabricated on High-Resistivity (HR) silicon substrates. After the bottom contact deposition, TiN barrier pads were patterned by e-beam lithography, in order to prevent the diffusion of Ni, which was deposited after this step. The CNTs growth was carried out by the CNT CVD equipment – Black Magic by Axitron, where the feeding gases were chosen to be NH_3 and C_2H_2 [12]. The growth of CNTs lasted 15 min at 650 °C with 650 V plasma voltage. The next step was the consecutive deposition of SiNx of total thickness of 200 nm taking place in two steps, where the process stopped for the removal of uncovered CNTs edges by plasma etching. The produced CNTs bunches had 100 nm height, the bunch diameter of 500 nm and 5 μm spacing between them which provide a direct comparison with the perspective samples of Au nanorods with the same dimensions (Fig. 1c). The MIM capacitors used had an area of 480x480μm^2.

2.3. Au nanorods

The last group of dielectric material used in present work was fabricated in practically three steps. A 100 nm SiNx layer was deposited with HF (13.56 MHz) PECVD method at 200 °C on bottom contact (CPW line for MEMS switches), which was deposited on SiO_2/high resistivity Si substrate. Holes with diameter of 500 nm were opened in the SiNx film and 100 nm Au nanorods were grown directly on the bottom contact. Finally, the nanostructured dielectric was covered with 100 nm PECVD SiNx (HF PECVD at 200 °C). The nanorods spacing was 5 μm and the capacitors area was also 480x480um^2, shown in Fig. 1b.

The MIM capacitors were assessed with current-voltage (I–V) characteristics in vacuum at 300 K with the aid of a Keithley 6487 source-meter/electrometer. The top electrode applied voltage was always positive to ensure electron injection from bottom electrode through the nanostructured film. The SiNx composition $x = \frac{N}{Si}$ for both CNTs bunches and Au nanorods was estimated to x = 1.25 while the randomly oriented CNTs base SiNx composition was found x = 1.22 [13].

The discharging process through the bulk material has been investigated with the aid of a single-point Kelvin Probe system [14], at room temperature and at ambient conditions. A polarization field with intensity of 1MV/cm has been applied for 20 min and the discharging process was monitored for 10^5 s. The charging conditions for MEMS with randomly oriented CNTs and Au nanorods where set to 2MV/cm for 40 min and 1.5MV/cm for 5 min respectively. The discharge process in MEMS capacitive switches has been monitored through the shift of up-state C−V characteristic towards pre-stress equilibrium.

3. Theoretical background

The introduction of nanostructured dielectric films in MEMS capacitive switches, although shown to provide better device performance

[9], has not been studied in depth. As already mentioned, the increase of charge draining through percolation has been discussed in [10] and initial assessment results of field emission in MEMS dielectric films with randomly oriented CNTs were demonstrated in [11,15].

In a nanostructured dielectric the measured current has to consider the basic charge transport mechanisms contributing through parallel paths [16]:

$$J = J_1 + J_2 + J_3 \quad (1)$$

where

$$J_1 = C_1 F exp\left(-\frac{q\varphi_1}{kT}\right) exp\left(\frac{qFr}{kT}\right) \exp\left(-\frac{r}{a}\right) \quad (2)$$

$$J_2 = C_2 F exp\left\{-\frac{q\left[\varphi_2 - \left(\frac{qF}{\pi\varepsilon_0\varepsilon_d}\right)^{\frac{1}{2}}\right]}{kT}\right\} \quad (3)$$

$$J_3 = C_3 F^2 exp\left(-\frac{E_3}{F}\right) \quad (4)$$

In this model J_1 is the hopping mechanism current, J_2 the contribution of Poole - Frenkel conduction and J_3 the Fowler – Nordheim (F–N) tunneling current, where C_1, C_2, C_3 are constants, $q\varphi_1$, $q\varphi_2$ the barrier height for each mechanism and α a constant that in most cases equals to Bohr radius.

In order to understand the impact of top layer on field emission it is essential to bear in mind that the coating of field emitters with a thin layer of certain wide band gap materials initially enhances emissivity. Increasing the thickness of the wide band gap material beyond a critical point, the emissivity of the coated emitter falls below that of the uncoated emitter [17,18]. Thus, the electrons can escape from the SiNx surface to a vacuum with greater ease than from the pristine CNT surface to a vacuum since the electron affinity of SiNx (~2 eV [19]) is lower than the work function of the CNTs ranging from 4.5 eV [20] to 5 eV [21].

For uncoated nanowires, Y. Chen et al., [17] have demonstrated that field emission may occur in vacuum for different CNT orientations. Extracting the data from Fig. 4 of [17] we present in Fig. 2 the Fowler-Nordheim plot which shows that for the parallel to substrate CNTs the field enhancement factor is larger.

4. Results and discussion

In MIM capacitors charge injection takes place under homogenous

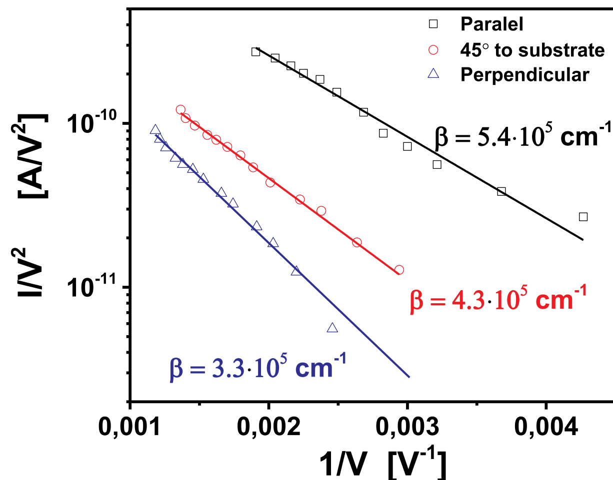

Fig. 2. F–N plot for CNTs for different orientations. Data obtained from Fig. 4 of [17].

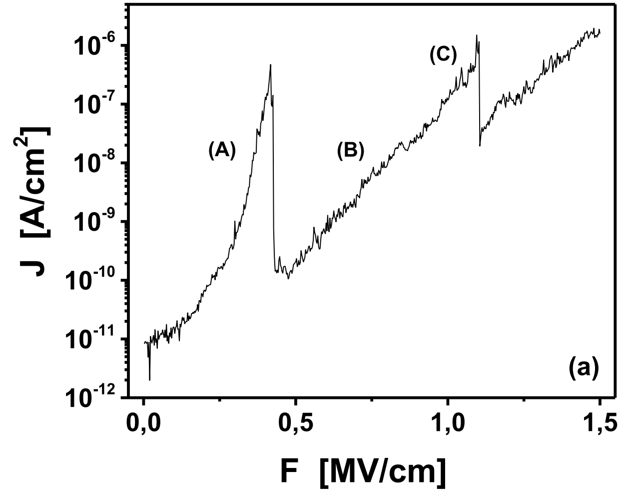

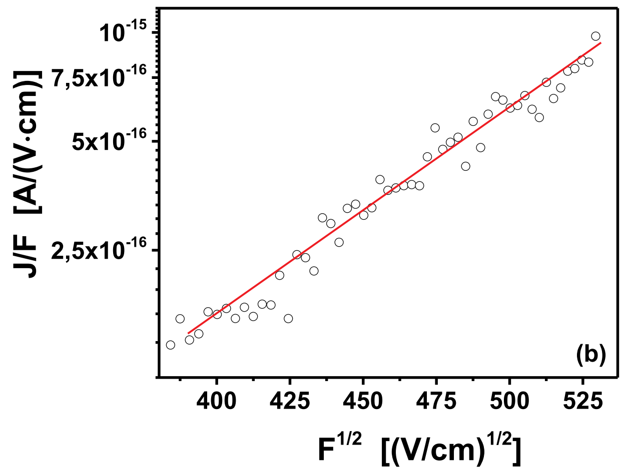

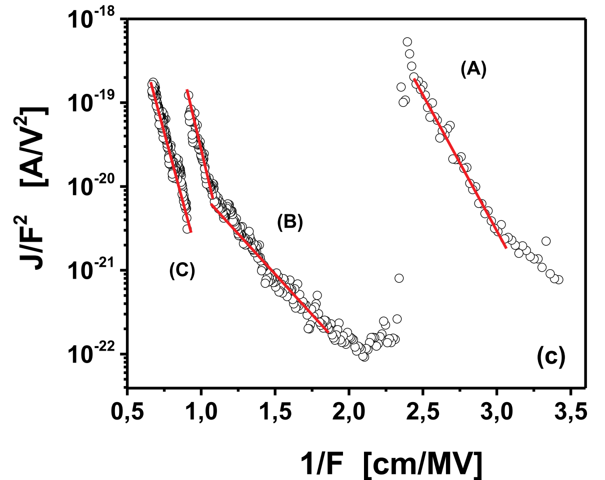

Fig. 3. (a) Ascending J-F characteristic, (b) Poole-Frenkel signature up to 250 kV/cm and (c) F–N plot in the range of 0.35-2MV/cm of the randomly oriented CNTs films.

electric field, generated from the parallel metal electrodes. However, the presence of nanoparticles in the lower half of dielectric films, used in this work, distorts the field homogeneity and the injected charges distribution.

In order to investigate the electrical properties of utilized nanostructured films MIM capacitors the results are separately discussed.

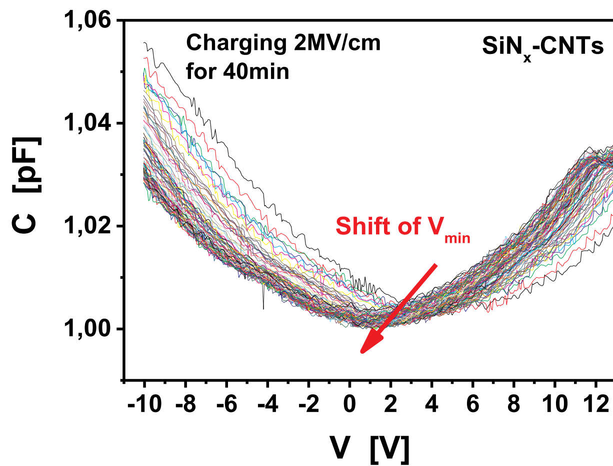

Fig. 4. Shift of V_{min} during discharging of the MEMS switches with randomly oriented CNTs.

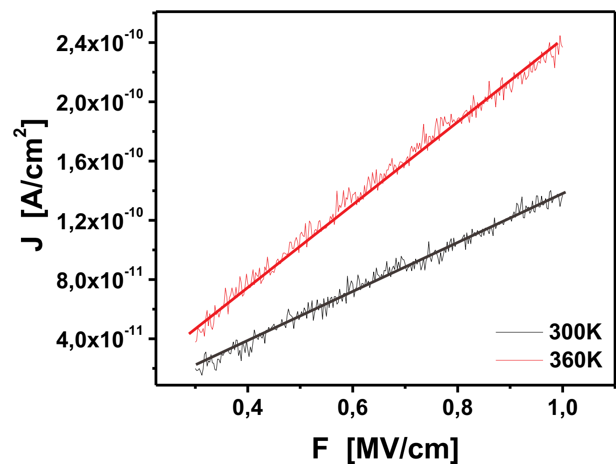

Fig. 5. Current-Voltage characteristic in MIM capacitors with vertically aligned CNT batches for different temperatures.

4.1. Assessment of randomly oriented CNTs

4.1.1. MIM capacitors

Fig. 3(a) shows a typical current-voltage characteristic obtained by applying fields up to 1.5MV/cm. The analysis of the ascending branch reveals the presence of field emission process arising from different sources. Particularly, for the ascend branch and for relatively low electric fields, up to 250 kV/cm, the contribution of Poole-Frenkel mechanism appears to be dominant Fig. 3(b). As applied bias increases a transition to field emission is observed, where the measured current increases rapidly Fig. 3(c). The non-continuous behavior of the F—N process has to be attributed to breakdown and CNTs loss [22] followed by contribution from CNTs with different field enhancement factor and emitting effective area.

These results clearly show the simultaneous presence of the two charge transport mechanisms while the hopping that was not detected cannot be excluded.

4.1.2. MEMS capacitive switches

Fig. 4 shows the shift of V_{min} during the discharging process of MEMS capacitive switches with randomly oriented CNTs. Further information about the device structure and experimental details can be found in [15]. In the later work, reference SiNx was compared with the nanostructured one and was found that MEMS switches with embedded randomly oriented CNTs provide faster discharging by an amount of 25%. The reported behavior was directly attributed to the presence of CNTs and the field-emission process, which also takes place during discharging. Furthermore, in the present work it is shown that due to the high electric fields generated by the CNTs the Poole-Frenkel mechanism also arises, thus the contribution of the combined transport mechanisms will provide faster charge draining from the bottom electrode.

4.2. Assessment of vertically aligned CNTs

The current-voltage characteristics in these nanostructured dielectrics show a different behavior. Primarily, no field emission is been observed (Fig. 5). The absence or very low field emission can be attributed to the electrostatic screening effect arising from the proximity of neighboring tubes and the large CNTs bunches diameter (500 nm) compared to their uniform length (100 nm) [23]. Calculations have shown that to minimize the screening effect the individual emitters should be evenly separated so that their spacing is greater than their height [24]. Furthermore, considering the fact that the nanotubes are close packed grown in bunches of 500 nm diameter, which corresponds to about 0.8% of the cell of dimension of 5 μm × 5 μm, we arrive to the conclusion that the measured current will arise from two regions, the empty of CNTs area with a field intensity of E and the bunch top area where the field is 2E, behaving like nanorods with properties described in [25].

The current-voltage characteristic (Fig. 5) does not comply with hopping or Frenkel-Poole mechanism. Instead of this, it exhibits a very good agreement with ohms law. Such a behavior although not encountered in silicon-nitride, it may not be excluded for the case of bulk limited conduction [26] in the presence of even a small number of carriers excited in the conduction or valence band. Ohmic like conductivity can be also obtained when hopping conduction occurs with very small hopping distance **r** although there are no evidences of such condition. Although not observed in the case of random oriented CNTs, this behavior has to be attributed to the presence of the vertically aligned CNTs and the SiNx deposition process. The same behavior is observed at elevated temperature (360 K). The fact that the conductivity increases with temperature leads to the conclusion that the mechanism is thermally activated. Based on these results we are led to the conclusion that further investigation is required for the understanding of transport mechanism and the possible implementation on charging mitigation.

4.3. Assessment of Au nanorods

4.3.1. MIM capacitors

As already mentioned above, the presence of nanorods modify the distribution of the electric field intensity at the top interface of the MIM capacitors and the value of (E_z) is determined by the height, diameter, spacing of the nanorods and the thickness of the overlaying dielectric film. In [25] a comparison between nanostructured nanorods of different spacing and diameters revealed that the interference of neighboring nanorods is negligible when the spacing extends over an area of about 400–500 nm from the center of each nanorod. This conclusion practically means that for the nanostructured material used in the present work with diameter of 500 nm and 5 μm spacing, the impact of the fringing field will be almost negligible. Hence, the current will be determined by both the local field intensity, the charge injection and the dominant transport mechanisms. Fig. 6 shows a typical current-voltage characteristic for electric fields up to 1MV/cm.

In SiNx the basic transport mechanisms, in absence of any contribution from field emission, are the hopping (Eq. (2)) and Frenkel-Poole (Eq. (3)). The first is usually encountered in low fields regime while the second in high fields regime. In such a dielectric film where the electric field intensity is not uniform, we assumed that Eq. (1)

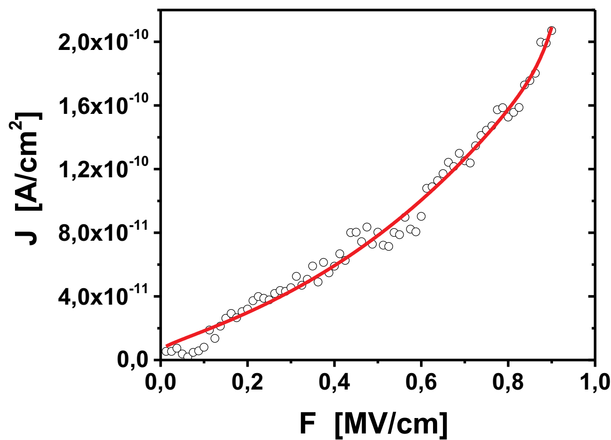

Fig. 6. Current-Voltage characteristic of Au nanorods MIMs. Fitted with the sum of hopping (Eq. (2)) and Poole-Frenkel (Eq. (3)).

contains only two terms and fitted the sum to experimentally obtained I-V characteristic (Fig. 6). Here it must be pointed out that the fitting results cannot be directly used to extract information on material properties but in contrary provides information on the physics on the charge transport processes in such a nanostructured dielectric film.

4.3.2. MEMS capacitive switches

Fig. 7 shows the shift of V_{min} during discharging of the MEMS switches with Au nanorods. In [25], a detailed comparison between the reference SiNx and nanostructured films with Au nanorods of different diameters and spacings revealed that discharging process in MEMS switches is almost 17% faster, a behavior that may attributed to the fact that Poole-Frenkel mechanism arises from relatively low electric field intensities.

4.4. Kelvin probe assessment

The decay of surface potential in a charged capacitive MEMS dielectric film and the top electrode in a charged MIM capacitor provide the information on the discharge process of dielectric film when the MEMS bridge is in up-state. In the present work the decay of surface potential is assessed with the aid of a single-point Kelvin Probe system [14], at room temperature and at ambient conditions. The method simulates the discharge process in a MEMS capacitive switch when the bridge can be still restored in the up-state. The results are presented in Fig. 8a for the random oriented CNTs and in Fig. 8b for the vertically aligned CNTs and Au nanorods that occupy only about 0.8% of nanostructure unit cell of 5 μm × 5 μm. The data of the corresponding reference materials are also included in each figure. Finally, the plots were normalized to initial potential in order to facilitate the comparison of the impact of the nanostructured material in the discharge process, which obviously increases the decay rate in these materials.

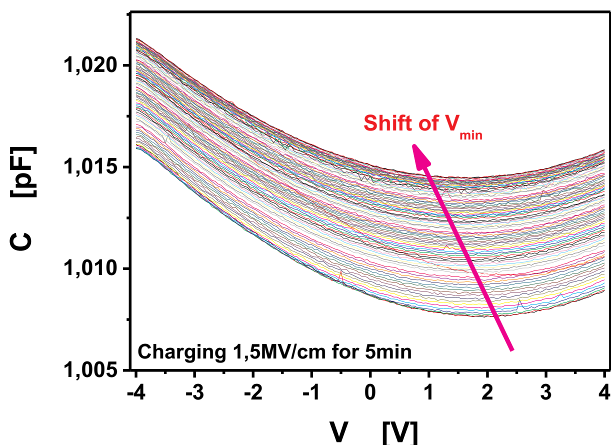

Fig. 7. Shift of V_{min} during discharging of the MEMS switches with Au nanorods.

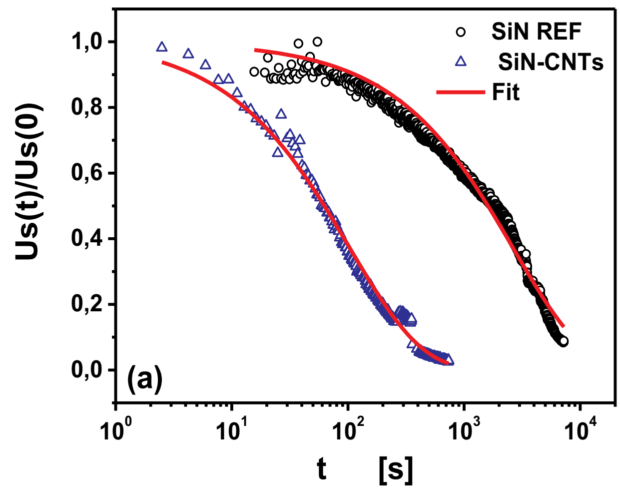

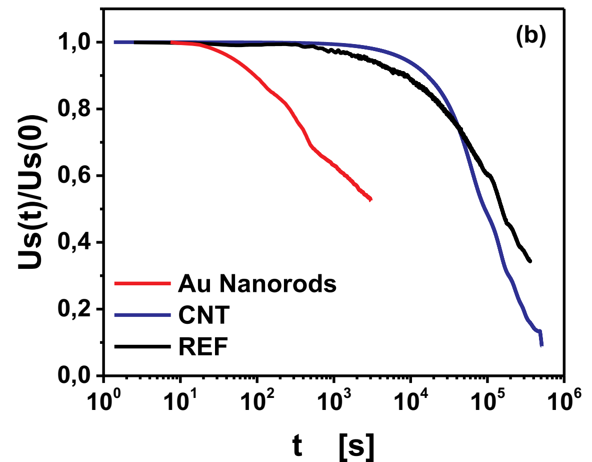

Fig. 8. Normalized surface potential decay with respect to the reference material for (a) randomly oriented CNTs, (b) vertically aligned CNTs and Au nanorods.

5. Conclusions

The electrical properties of SiNx with embedded CNTs, of random orientation or vertically aligned bunches, and Au nanorods have been investigated. It is found that the electrical properties are significantly affected by both the embedded nanofiller and the orientation. Thus, in the case of random oriented CNTs the transport mechanisms are Frenkel-Poole and field emission at low and high electric fields respectively. In the case of Au nanorods, the hopping and Frenkel-Poole mechanisms are detected at low and high electric fields respectively. Finally, for vertically aligned CNTs the current-voltage characteristic is found to follow ohm's law, leading to the conclusion that this material requires further investigation. The discharge rate through the bulk material is found to increase with the addition of nanofillers. It is important to notice that the discharge rate depends on the host material deposition conditions and the organization of the nanofillers. Furthermore, it is important to notice that for the vertically aligned nanostructures their density plays a crucial role on the discharge process. Moreover, for the vertically aligned bunches of CNTs the screening

effect does not allow the manifestation of field emission and therefore the benefits of isolated CNTs. Considering the thermal stress on Si substrate during CNTs growth and the potential presence of thermal donors in the substrate we are led to the conclusion that all proposed nanostructured materials can be implemented in MEMS with the randomly orientated CNTs representing the lower cost and easy optimization followed by the higher cost Au nanorods reinforced material. The vertically aligned CNT bunches requires rigorous optimization in both the growth temperature and the understanding the resulting material electrical properties.

Acknowledgements

This work is partially co-financed by Greece and the European Union (European Social Fund-ESF) through the Operational Programme «Human Resources Development, Education and Lifelong Learning» in the context of the project "Strengthening Human Resources Research Potential via Doctorate Research" (MIS-5000432), implemented by the State Scholarships Foundation (IKY). Also has been co-financed by the European Union and Greek national funds through the Operational Program Competitiveness, Entrepreneurship and Innovation, under the call RESEARCH – CREATE – INNOVATE (Project code: T1EDK-00329).

References

[1] G.M. Rebeiz, RF MEMS: Theory, Design, and Technology, J. Willey and Sons, Hoboken, 2004.
[2] M. Koutsoureli, N. Siannas, G. Papaioannou, Temperature accelerated discharging processes through the bulk of PECVD silicon nitride films for MEMS capacitive switches, Microelectron. Reliab. 76–77 (2017) 631–634.
[3] M. Koutsoureli, N. Tavassolian, G. Papaioannou, J. Papapolymerou, Dielectric charging in capacitive microelectromechanical system switches with silicon nitride, Appl. Phys. Lett. 98 (9) (2011).
[4] G. Papaioannou, M.-N. Exarchos, V. Theonas, G. Wang, J. Papapolymerou, Temperature study of the dielectric polarization effects of capacitive RF MEMS switches, IEEE Trans. Microwave Theory Tech. 53 (11) (2005) 3467–3473.
[5] J. Robertson, Electronic structure of silicon nitride, Philos. Mag. B 63 (1) (1991/01/01 1991) 47–77.
[6] M. Koutsoureli, E. Papandreou, L. Michalas, G. Papaioannou, Investigation of silicon nitride charging, Microelectron. Eng. 90 (2012) 145–148.
[7] R. Daigler, E. Papandreou, M. Koutsoureli, G. Papaioannou, J. Papapolymerou, Effect of deposition conditions on charging processes in SiNx: application to RF-MEMS capacitive switches, Microelectron. Eng. 86 (3) (2009) 404–407.
[8] U. Zaghloul, G. Papaioannou, F. Coccetti, P. Pons, R. Plana, Dielectric charging in silicon nitride films for MEMS capacitive switches: effect of film thickness and deposition conditions, Microelectron. Reliab. 49 (9) (2009) 1309–1314 2009/09/01/.
[9] C. Bordas, et al., Carbon nanotube based dielectric for enhanced RF MEMS reliability, 2007 IEEE/MTT-S International Microwave Symposium, 2007, pp. 375–378.
[10] G. Papaioannou, L. Michalas, M. Koutsoureli, S. Bansropun, A. Gantis, A. Ziaei, Charging mechanisms in nanostructured dielectrics for MEMS capacitive switches, 2014 IEEE 14th Topical Meeting on Silicon Monolithic Integrated Circuits in Rf Systems, 2014, pp. 98–100.
[11] D. Birmpiliotis, G. Stavrinidis, G. Konstantinidis, G. Papaioannou, Temperature accelerated discharging process in SiNx films with embedded CNTs for applications in MEMS switches, 2018 Symposium on Design, Test, Integration & Packaging of MEMS and MOEMS (DTIP), IEEE, 2018, pp. 1–6.
[12] L. Xu, et al., Effect of substrates and underlayer on CNT synthesis by plasma enhanced CVD, Adv. Manuf. 1 (3) (2013) 236–240.
[13] S. Habermehl, R.T. Apodaca, R.J. Kaplar, On dielectric breakdown in silicon-rich silicon nitride thin films, Appl. Phys. Lett. 94 (1) (2009).
[14] Kelvin Probe Information Site, Available http://www.kelvinprobe.info/.
[15] M. Koutsoureli, G. Stavrinidis, D. Birmpiliotis, G. Konstantinidis, G. Papaioannou, Electrical properties of SiNx films with embedded CNTs for MEMS capacitive switches, Microelectron. Reliab. 76–77 (2017) 614–618 2017/09/01/.
[16] S.M. Sze, Current transport and maximum dielectric strength of silicon nitride films, J. Appl. Phys. 38 (7) (1967) 2951–2956.
[17] Y. Chen, D.T. Shaw, L. Guo, Field emission of different oriented carbon nanotubes, Appl. Phys. Lett. 76 (17) (2000) 2469–2471.
[18] W. Yi, et al., Field-emission characteristics from wide-bandgap material-coated carbon nanotubes, Adv. Mater. 14 (20) (2002) 1464–1468.
[19] S.X. Tao, A. Theulings, J. Smedley, H. van der Graaf, DFT study of electron affinity of hydrogen terminated β-Si3N4, Diamond and Related Materials, 53 2015, pp. 52–57 2015/03/01/.
[20] W.S. Su, T.C. Leung, C.T. Chan, Work function of single-walled and multiwalled carbon nanotubes: first-principles study, Phys. Rev. B 76 (23) (2007).
[21] S. Suzuki, Y. Watanabe, Y. Homma, S. Fukuba, S. Heun, A. Locatelli, Work functions of individual single-walled carbon nanotubes, Appl. Phys. Lett. 85 (1) (2004) 127–129.
[22] M. Wang, L.-M. Peng, J. Wang, Q. Chen, Electron field emission characteristics and field evaporation of a single carbon nanotube, J. Phys. Chem. B 109 (1) (2005) 110–113.
[23] L. Nilsson, et al., Scanning field emission from patterned carbon nanotube films, Appl. Phys. Lett. 76 (15) (2000) 2071–2073.
[24] D. Biswas, R. Rudra, Shielding effects in random large area field emitters, the field enhancement factor distribution, and current calculation, Phys. Plasmas 25 (8) (2018) 083105.
[25] M. Koutsoureli, et al., Electrical properties of nanostructured SiN films for MEMS capacitive switches, J. Micromech. Microeng. 27 (1) (2017) 014001.
[26] F.-C. Chiu, A review on conduction mechanisms in dielectric films, Adv. Mater. Sci. Eng. 2014 (2014) 1–18.

Microelectronic Engineering 223 (2020) 111230

Contents lists available at ScienceDirect

Microelectronic Engineering

journal homepage: www.elsevier.com/locate/mee

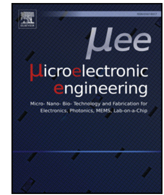

Research paper

Thermally activated discharging mechanisms in SiN_x films with embedded CNTs for RF MEMS capacitive switches

M. Koutsoureli[a,*], G. Stavrinidis[b], D. Birmpiliotis[a], G. Konstantinidis[b], G. Papaioannou[a]

[a] Section of Condensed Matter Physics, National and Kapodistrian University of Athens, Athens 15784, Greece
[b] IESL –FORTH, GR-71110 Heraklion, Greece

ARTICLE INFO

Keywords:
RF MEMS switches
Dielectric charging
Nanostructured dielectrics
Silicon nitride

ABSTRACT

In the present work, we investigate thermally activated processes in nanostructured SiN_x films with embedded CNTs, which can be used in RF MEMS capacitive switches. Nanostructured films have been fabricated with a simple process, in order to incorporate CNTs on the lower SiN_x layer and a reference SiN_x material has been also fabricated with the same method (without CNTs), in order to compare the properties of the nanostructured films with the pristine material. Thermally stimulated depolarization currents (TSDC) assessment and a single-point Kelvin Probe (KP) system have been used in MIM capacitors, in order to investigate the electrical properties of the utilized films.

The nanostructured material is found to exhibit lower charging and smaller discharging time, which makes it a promising candidate for RF MEMS capacitive switches. Thermally activated discharging mechanisms have been identified and the presence of CNTs is found to diminish a discharging mechanism with a characteristic time larger than five days at room temperature. Different discharging mechanisms are identified and distinguished for the first time, to the best of our knowledge, between a reference and a nanostructured SiN_x dielectric film. Charge displacement in the bulk material during discharge takes place through hopping processes and larger mean hopping distance and zero field conductivity has been found in the nanostructured films. The reduction of the discharge characteristic time and the simultaneous suppression of trapping centers in the films with embedded CNTs indicate a direct relation between the macroscopic electrical properties and the microscopic defects in the dielectric material.

1. Introduction

RF MEMS (Radio-Frequency Micro-Electro-Mechanical-System) capacitive switches are promising devices for several applications, since they possess many benefits over conventional electronics switches [1], but they have not yet reached commercialization due to reliability problems [1]. The use of nanocomposite dielectric films has been proposed as a solution to eliminate dielectric charging [2–6], a persistent reliability issue of these devices [1,7,8]. Especially, the use of nanostructured silicon nitride (SiN_x) dielectric films seems to be quite promising. In order to increase the charge draining through the bottom electrode C. Bordas et al. [2] deposited a two layer SiN_x, the top of which included carbon nanotubes (CNTs) of various concentrations. The paper reported a huge increase of the dielectric material "Figure of Merit" with increasing the CNTs concentration. The latter was translated into a several orders of magnitude improvement of the MEMS lifetime [2]. Moreover, the effect of CNTs geometry on tunneling assisted electrical network in nanocomposites has been presented in [6,9]. The electrical properties of SiN_x films with gold nanorod arrays and the performance of MEMS capacitive switches with these films has been in depth analyzed in [3,10,11].

Considering the fact that the charging and discharging are thermally activated processes [12–15], the present work aims to provide a better insight on the electrical properties of nanostructured SiN_x films with embedded CNTs, by studying the effect of temperature on the discharging processes through the bulk material and through the injecting contacts. Reference SiN_x films have been also fabricated and tested in order to compare their characteristics with the nanostructured material. The experimental results revealed a significant decrease of the discharging time in the nanostructured material and the suppression of a charging contribution which exhibits a characteristic time, at room temperature, similar to the discharging time constant of the reference material. Finally, the presence of CNTs are found to alter the percolation paths by increasing the mean hopping distance and the zero field

* Corresponding author.
E-mail address: mkoutsoureli@phys.uoa.gr (M. Koutsoureli).

https://doi.org/10.1016/j.mee.2020.111230
Received 18 November 2019; Received in revised form 20 January 2020; Accepted 21 January 2020
Available online 22 January 2020
0167-9317/ © 2020 Elsevier B.V. All rights reserved.

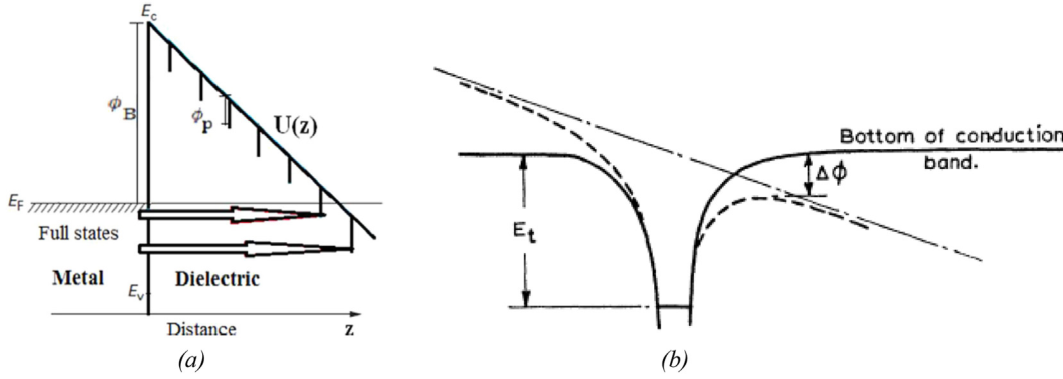

Fig. 1. (a) TAT injection [18] and (b) Mechanism of Poole-Frenkel effect [21].

conductivity in the nanostructured films.

2. Theoretical background

2.1. Charging process

The charging of SiN_x films in a MIM (Metal-Insulator-Metal) capacitor is achieved when an electric field is applied across the metal electrodes and it takes place through two basic processes [16–18]:

i) Trap Assisted Tunneling (TAT) which is responsible for charge injection from the metal electrodes into the dielectric film and
ii) Poole-Frenkel mechanism that dominates charge redistribution in the bulk of the dielectric material. This mechanism appears on condition that the applied electric field is strong while for low electric fields charge transport in the bulk material is expected to take place through the hopping mechanism [19].

TAT current is generated by carriers in the metal electrode, which are transferred to dielectric traps by the tunneling effect (Fig. 1a). The TAT current density can be written as [20]:

$$J_{TAT}(t) = e\int_{x=0}^{\infty}\int_{E_t=-\infty}^{-eFx} N(x,E_t)\bullet(f_\infty - f_0)\bullet\frac{e^{-t/\tau}}{\tau}\bullet\frac{x}{L}\bullet dE_t\bullet dx \tag{1}$$

where e is the electronic charge, L is the thickness of the dielectric film, x and E_t are respectively the spatial location away from the electrode into the dielectric and the energy level of the trap measured down from the conduction band edge of the dielectric at $x = 0$. $N(x,E_t)$ is the trap distribution function in the presence of an electric field F and it is in units of per unit volume per unit energy. Parameter τ is given by: $\tau = \tau_0\bullet exp\left(\frac{2x\sqrt{2m\mid E_t\mid}}{\hbar}\right)$, where τ_0 is the lower limit of tunneling relaxation times, related to electron capture cross section, m is the electronic mass and $\hbar$ the Plank's constant. Finally, f_0 and f_∞ are the Fermi functions: $f_0(x,E_t) = \left\{1 + exp\left(\frac{E_t + eFx - E_F}{k_B T}\right)\right\}^{-1}$ and $f_\infty(E_t) = \left\{1 + exp\left(\frac{E_t - E_F}{k_B T}\right)\right\}^{-1}$, with k_B being the Boltzmann's constant, T the temperature and E_F the Fermi energy of the metal electrode.

The Poole-Frenkel effect, or field-assisted thermal ionization, is the lowering of a Coulombic potential barrier when it interacts with an electric field, as shown in Fig. 1b. The current density of this mechanism is given by [21]:

$$J_{PF} = \sigma_{PF}\bullet F\bullet exp\left(\frac{-e\left(E_t - \sqrt{\frac{eF}{\pi\varepsilon_0\varepsilon_r}}\right)}{k_B T}\right) \tag{2}$$

where σ_{PF} is the Poole-Frenkel conductivity, E_t is the trap energy, F is the intensity of the electric field, ε_0 is vacuum permittivity and ε_r is the dielectric constant.

2.2. Discharging process

The discharging process of SiN_x films that are used in RF MEMS capacitive switches usually takes place under the presence of low electric fields [3,22], where hopping dominates charge transport.

Hopping conduction is due to the tunneling effect of trapped electrons "hopping" from one trap site to another in dielectric films [23–27]. According to the calculations of R. M. Hill [24] as well as M. Pollak and I. Riess [26], in the case of moderate electric fields (i.e. when $F < \frac{2k_B T}{ae}$, where α is the Bohr radius of the localized states), the expression of hopping conduction is:

$$J_{hop}(F) = \sigma_H\bullet F\bullet exp\left[\frac{eGr_m F}{k_B T}\right] \tag{3}$$

where J_{hop} is the current density, F is the electric field and r_m is the mean hopping length on the percolation paths. G is a constant, the value of which was determined to be 0.17 by M. Pollak and I. Riess [26] and 0.85 by R. M. Hill [24], a difference that can be attributed to different percolation procedures followed in each work. Parameter σ_H represents zero field conductivity, which is proportional to mean hopping length according to [27,28].

In a MIM capacitor, the surface potential (U_S) of the top electrode at time t can be written in the form:

$$U_S(t) = \frac{Q(t)}{C} = \frac{d}{\varepsilon_r\varepsilon_0}\bullet\sigma(t) \tag{4}$$

where C represents the capacitance, d is the film thickness, Q and σ represent the charge and the charge density respectively of the image charges that appear in the plates of the capacitor. According to these, the average net discharge current density is given by:

$$J_{disch}(t) = -\frac{d\sigma(t)}{dt} = -\frac{\varepsilon_r\varepsilon_0}{d}\bullet\frac{dU_S(t)}{dt} \tag{5}$$

Thus, when hopping dominates the discharging process, the current J_{disch} will be equal to J_{hop} and taking into account Eqs. (3) and (5), we obtain the following expression:

$$t = -\frac{\varepsilon_r\varepsilon_0}{\sigma_H}\bullet\int_{U_{S,0}}^{U_S}\frac{dU_S}{U_S\bullet exp\left(\frac{eGr_m\bullet U_S}{dk_B T}\right)} \tag{6}$$

which associates the discharging time with the value of surface potential.

3. Experimental details

A simple fabrication process has been adopted for the deposition of both the nanostructured and reference films. The SiN_x films were grown

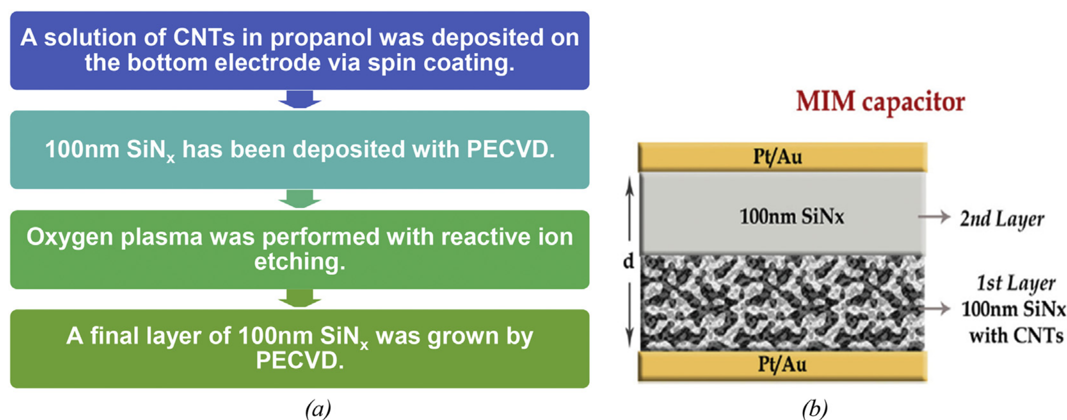

Fig. 2. (a) The steps of the deposition process for the nanostructured dielectric films and (b) a schematic of utilized MIM capacitors with nanostructured film.

with high frequency (13.5 MHz) Plasma Enhanced Chemical Vapor Deposition (PECVD) method under a substrate temperature of 300 °C. The deposition procedure was performed in two steps simultaneously, for both the nanostructured (SiN_x/CNTs) and reference (REF) materials, a block diagram is shown in Fig. 2a. CNTs with 1 nm diameter and a length of 2-3 μm was first deposited over the bottom Pt/Au electrode, by using a spinner at a frequency of 1000 rpm. The CNTs were embedded in a first SiN_x layer, of 100 nm thickness, deposited by PECVD, aiming to improve the charge draining by the bottom electrode. Oxygen plasma was then performed by reactive ion etching, in order to shorten CNTs that protruded the first SiN_x layer. Finally, the deposition of a second 100 nm SiN_x layer on top took place by PECVD (Fig. 2b) to increase the breakdown voltage and the top Pt/Au electrode has been deposited. We mention that since the length of the incorporated CNTs is larger than the thickness of the first 100 nm SiN_x layer, the CNTs are expected to be distributed with random orientation in this layer. In addition, we state that the density of CNTs in the nanostructured film was $3\frac{CNTs\ number}{10\ \mu m^2}$.

The material assessment was performed with symmetrical metal contacts (Pt/Au) MIM capacitors. The bottom contact was common for all capacitors while the top one had 1 mm diameter and the thickness of the dielectric film was 200 nm (Fig. 2b). The diameter of top contact was much larger than the film thickness, in order to minimize the effect of lateral charge diffusion.

A single-point Kelvin Probe (KP020) [29] system has been used to monitor the decay of top electrode potential during discharge at different temperatures (300 K – 400 K). The potential decay was monitored for a time length up to several days, while charging was performed by applying an electric field of 1MV/cm for 20 min at each temperature.

Thermally stimulated depolarization currents (TSDC) technique has been also used in order to investigate thermally activated mechanisms in the films. The TSDC method allows the monitoring and analysis of contributing thermally activated charging mechanisms, although the trapped charges are collected by the injecting electrodes [30]. Thus, by ramping temperature the TSDC method allows the observation of very slow charging mechanisms, non-observable at room temperature through isothermal discharge currents. The TSDC current has been measured with the aid of a Keithley 6487 voltage source – picoampere meter by ramping temperature from 200 K to 450 K, with a heating rate of 2.5 K/min. In the case of TSDC assessment, the charging field was 1MV/cm and it was applied at 450 K for 20 min.

It is important to state that during all experiments the charging level was maintained low in order to understand the dependence of the discharging process on the material properties and prevent device degradation arising from high charging levels.

4. Results and discussion

The discharge process has been investigated with the aid of KP method at different temperatures, in order to examine thermally activated processes. The use of MIM capacitors screens any non-uniform charge distribution due to the presence of the top electrode, and the top electrode potential arises from a uniform charge distribution that is practically the same with the mean charge density calculated from the bias shift of up-state C-V characteristic minimum in RF MEMS capacitive switches [31].

KP measurements, performed at 300 K for both REF and SiN_x/CNTs materials, revealed that nanostructured films exhibit a much faster discharge process (Fig. 3), since the calculated characteristic discharging time is almost two orders of magnitude smaller than the corresponding time of REF films, a result that comes along with our previous work presented in [4].

The decay of surface potential has been found to obey a stretched exponential law of the form:

$$U_S(t) = U_{S,0} \bullet exp\left[-\left(\frac{t}{\tau}\right)^{\beta}\right] \tag{7}$$

where $U_{S,0}$ is the surface potential immediately after charging (i.e. at $t = 0$ s), τ is the characteristic time of the discharging process and β is the stretched exponential factor, with $0 < \beta < 1$. The stretched-exponential or Kohlrausch-Williams-Watts function, described by Eq. (7), has been widely used in the description of a large variety of relaxation phenomena in condensed matter physics [32], providing a macroscopic description of the relaxation of many physical complex systems.

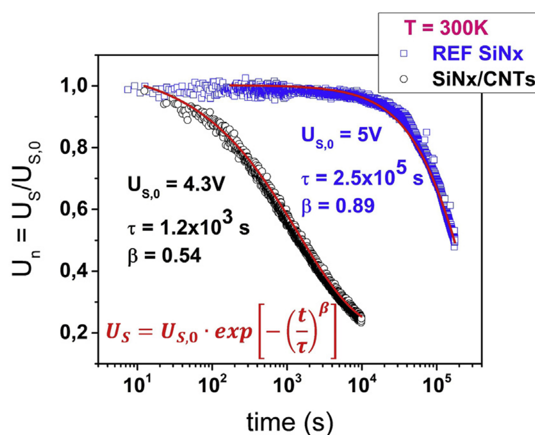

Fig. 3. Normalized values of surface potential decay during discharge, for samples with REF SiN_x and SiN_x/CNTs films, measured with KP system at 300 K. Fitting performed with Eq. (7).

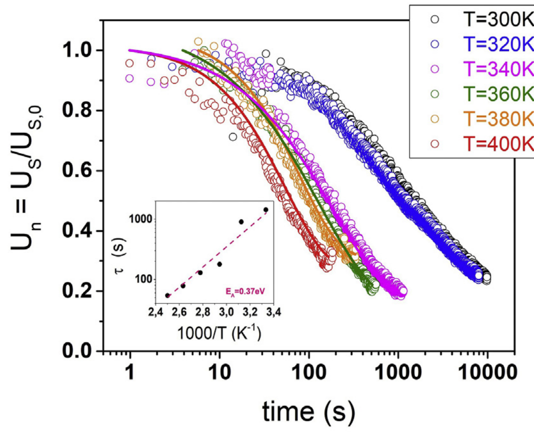

Fig. 4. Normalized values of surface potential decay during discharge, for samples with SiN_x/CNTs films, measured with KP system at various temperatures and fitting of experimental data with Eq. (7) (lines in the figure). Inset: Arrhenius plot of the characteristic time for the discharge process.

The acceleration of the discharging process in SiN_x/CNTs films is due to the presence of CNTs that are embedded in the lower half and are expected to assist the charge drain towards the bottom metal contact. Moreover, due to the random orientation of CNTs, there will be larger "variety" of charges' conduction paths during discharge. All these could explain the smaller value of parameter β (Fig. 3) on the nanostructured material, which implies a larger degree of complexity on the discharge process in this system. Finally, the value of $U_{S,0}$ is found to be smaller in nanostructured films, for the same charging conditions, which implies that charging is expected to be lower in these films.

The discharge process through the bulk material has been also found to be thermally activated (Fig. 4), with the characteristic discharging time following Fröhlich law [30]:

$$\tau = \tau_0 \bullet exp\left(\frac{E_A}{k_B T}\right) \tag{8}$$

where $\tau_0 = 9.4 \times 10^{-4}$s is the characteristic time at infinite temperature (τ_0^{-1} is the characteristic frequency factor and is related to the vibrational frequency of the material) and $E_A = 0.37$ eV is the activation energy in the nanostructured material. On the reference material, likewise, it has been found that $\tau_0 = 3 \times 10^{-4}$s and $E_A = 0.53$ eV.

An additional approach has been adopted in order to gain a better insight on the mechanism of charge transport through the bulk material of the utilized dielectric films, by assuming hopping transport and simulating the decay with Eq. (6) (Fig. 5). The value of surface potential during discharge, measured with KP system at each temperature on SiN_x/CNTs films, was smaller than 5 V (e.g. see values of $U_{S,0}$ at Fig. 3), a value that corresponds to an electric field lower than 500 kV/cm, fact that justifies the assumption of hopping conduction. Hopping transport in the discharge process has been also reported in PECVD SiN_x films for RF MEMS capacitive switches by Koutsoureli et al. in [3,33].

Fig. 5 shows safisfactory results obtained from fitting the experimental data with Eq. (6) for samples with REF and SiN_x/CNTs films, fact that implies that hopping is the dominant conduction mechanism during discharge in both films. It is important to mention that the CNTs presence will generate larger average charging field intensity in the nanostructured films than in the reference material, although the same electric field is applied across the metal electrodes of MIM samples during charging. This is expected to affect the distribution of the injected charges, according to theoretical models proposed in [16–18], since as the intensity of the electric field increases the centroid of the injected charge distribution is shifted deeper in the film. The latter, with the simultaneous presence of CNTs on the lower half of the nanostructured films, is expected to generate a stronger electric field during discharge, which arises from the trapped charges. This is expected to alter the percolation paths of the discharging process between nanostructured and reference materials, according to Pollak and Riess [26], fact that is confirmed from the fitting of the experimental data with Eq. (6), which showed that the nanostructured material exhibits a larger value of parameter $L \equiv Gr_m$ and larger zero field conductivity, σ_H.

On the following, thermally activated discharging mechanisms have been further investigated with the aid of TSDC method. TSDC spectra of nanostructured and REF materials are shown in Fig. 6. Taking into account that the current density, J_{TSDC}, produced by the progressive decrease in polarization in the course of a TSDC experiment, where time and temperature vary simultaneously can be approximated by [30]:

$$J_{TSDC}(T) \approx \frac{P_S(T_p)}{\tau_0} exp\left(-\frac{E_A}{k_B T}\right) exp\left[-\frac{1}{\gamma\tau_0}\bullet\frac{k_B T^2}{E_A}\bullet exp\left(-\frac{E_A}{k_B T}\right)\right] \tag{9}$$

where T_p is the polarization temperature, γ is the heating rate and P_S the steady state polarization, we have fitted the experimental data with Eq. (9), assuming that there are two major contributing discharging mechanisms. It has been then found that in SiN_x/CNTs films the first mechanism has an activation energy of $E_{A,1} = 0.25$ eV and the second one has $E_{A,2} = 0.30$ eV (Fig. 6). For REF material, the corresponding values of each mechanism (inset of Fig. 6) are $E'_{A,1} = 0.18$ eV and $E'_{A,2} = 0.31$ eV. Thus, the presence of CNTs seems to influence mainly the first mechanism, which appears on the high temperature region.

In addition, the total charge density collected in the external circuit

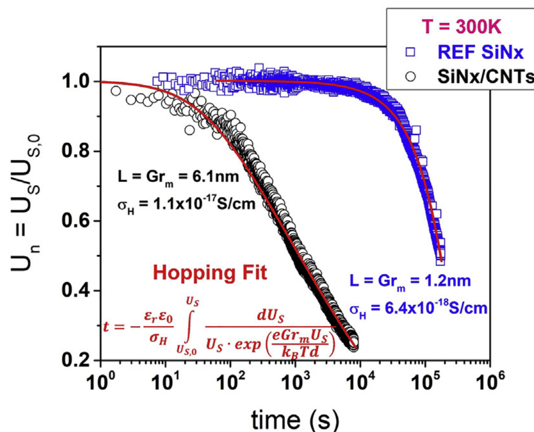

Fig. 5. Fitting of normalized values of surface potential decay at 300 K, using Eq. (6), on SiN_x/CNTs and SiN_x REF films. Fitting parameters are also shown.

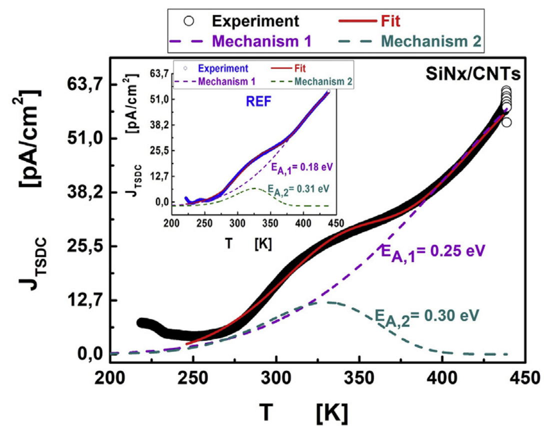

Fig. 6. TSDC spectrum of MIM with SiN_x/CNTs film and its analysis with two contributing discharging mechanisms, using Eq. (9). Inset: Analysis of TSDC spectrum for REF material.

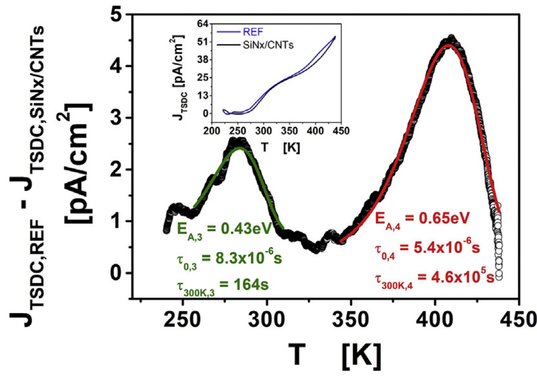

Fig. 7. TSDC spectra subtraction for REF and SiN_x/CNTs films and its analysis, using Eq. (9), at high and low temperatures region. Inset: TSDC spectra for samples with REF and SiN_x/CNTs films.

during temperature scan (from $T_1 = 200$ K to $T_2 = 440$ K) was calculated by integration over the TSDC spectra [30]:

$$\sigma_{TSDC} = \frac{1}{\gamma} \int_{T_1}^{T_2} J_{TSDC}(T)dT \tag{10}$$

and found equal to 1.02×10^{-7}C/cm^2 and 1.25×10^{-7}C/cm^2 for SiN_x/CNTs and REF films respectively, i.e. there is 8% decrease in nanostructured films. This behavior can be attributed to the fact that the average value of the electric field during charging is expected to be larger in SiN_x/CNTs material, as already mentioned. Thus, there will be an enhancement of charge redistribution in the bulk of nanostructured films through Poole-Frenkel processes, which shifts the centroid of the injected charge distribution deeper in the films and translates to lower dielectric charging.

On the following, in order to have a clearer view on the effect of CNTs in the nanostructured material, we compared TSDC spectra in REF and SiN_x/CNTs films. We have thus determined the difference between the measured discharging current on REF material and the corresponding values on SiN_x/CNTs material. As it is shown on Fig. 7, there is a discrete discharging mechanism in REF material on the low temperature regime ($T < 300K$), that is not present on the nanostructured film. By fitting the experimental data with Eq. (9), at low temperatures regime, we have determined the activation energy of the above-mentioned mechanism: $E_{A,3} = 0.43$ eV and its characteristic time at infinite temperature: $\tau_{0,3} = 8.3 \times 10^{-6}$s. The charge collected in the external circuit due to this mechanism has been found equal to 3.4×10^{-9}C/cm^2. However, the characteristic time of this mechanism at 300 K is found quite small: $\tau_{300K,3} = 164$ s (using Eq. (8)) and therefore, it is not expected to contribute significantly to the device lifetime.

Apart from the mechanism that appears at low temperatures, there is also another discharging mechanism at high temperatures ($T > 350$ K), which has been also analyzed using Eq. (9). The charge collected in the external circuit due to this mechanism has been found equal to 7.2×10^{-9}C/cm^2, its activation energy is $E_{A,4} = 0.65$ eV and $\tau_{0,4} = 5.4 \times 10^{-6}$s. The characteristic time of this mechanism will obey Eq. (8) and thus at 300 K we obtain: $\tau_{300K,4} = 4.6 \times 10^5$s, a value which is larger than five days' time.

The above-mentioned mechanisms (Mechanisms 3 and 4) that have been identified from TSDC spectra subtraction can be observed only in REF and not in SiN_x/CNTs films. Thus, the presence of CNTs in the nanostructured material seem to diminish them.

It is important to mention that this is the first time, to the best of our knowledge, that different discharging mechanisms have been identified and distinguished, between a reference and a nanostructured SiN_x dielectric film.

In order to have a better view on the identified discharging mechanisms we present the obtained results from KP and TSDC assessments on Table 1. We mention that parameter σ in this table stands for the equivalent surface charge distribution in KP method (see Eq. (4)) while in TSDC it is the charge that would have been measured in the external circuit for each mechanism (see Eq. (10)). The characteristic time of each mechanism has been determined and presented for 300 K (τ_{300K}), taking into account Eq. (8). Finally, the characteristics of the two mechanisms that have been identified in REF samples from TSDC spectra subtraction (Fig. 7) are presented on the two last columns of Table 1 (Mechanisms 3 and 4).

Regarding Mechanisms 1 and 2, they exhibit smaller τ_{300K} and lower σ in the nanostructured material. Mechanism 3 has been identified in REF material from TSDS assessment and it is possible that the same mechanism will be present in other PECVD SiN_x materials that exhibit a characteristic discharging time in the order of 10^2s, at room temperature. More specifically, E. Papandreou et al. in [34] have identified a discharging mechanism with an activation energy of about 0.4 eV and a characteristic time of $\sim 10^2$s, at room temperature, for a variety of SiN_x films that have been fabricated with different deposition conditions. Moreover, it is remarkable to mention that in REF material, τ_{300K} obtained from KP measurement is of the same order of magnitude with the corresponding value of Mechanism 4, obtained from TSDC, although there is a small difference on the values of the obtained activation energy. The values of parameter σ also differ a lot (almost two orders of magnitude). In order to understand these, one should bear in mind that in KP method, the measured surface potential decay arises only from charge displacement through the bulk material and towards the bottom electrode. In TSDC assessment, on the contrary, the measured discharge current arises from the algebraic sum of the charge flowing towards the injecting contacts and the charge flowing through the dielectric film, where carrier recombination takes place, and collected by the opposite contacts [30]. So, the charge collected during temperature scan in TSDC is expected to be lower in magnitude than the equivalent surface charge density determined immediately after charging from KP method. Mechanism 4 is thus believed to play a significant role in charge displacement through the bulk of reference material, while the presence of CNTs result to its disappearance. Taking into account that the discharging process in the dielectric films of RF MEMS capacitive switches takes place during the pull-up state of the switch, where the injected charges are transported through the bulk of the dielectric material, it is obvious that the diminishment of Mechanism 4 due to the presence of

Table 1
The characteristics of the identified mechanisms in utilized films, obtained from KP and TSDC methods.

		KP	TSDC			
			Mechanism 1	*Mechanism 2*	*Mechanism 3*	*Mechanism 4*
REF	E_A (eV)	0.53	0.18	0.31	0.43	0.65
	τ_{300K} (s)	2.5×10^5	7.3×10^4	3.2×10^3	164	4.6×10^5
	σ (C/cm^2)	$< 1.7 \times 10^{-7}$	1.1×10^{-7}	1.5×10^{-8}	3.4×10^{-9}	7.2×10^{-9}
SiN_x/CNTs	E_A (eV)	0.37	0.25	0.30	–	–
	τ_{300K} (s)	1.2×10^3	5.5×10^4	2.2×10^3	–	–
	σ (C/cm^2)	$< 1.3 \times 10^{-7}$	9.1×10^{-8}	1.1×10^{-8}	–	–

CNTs will increase device reliability.

Taking all these into consideration, we conclude that nanostructured films have shown lower charging, faster discharging and the presence of CNTs diminishes a discharging mechanism of reference material (Mechanism 4), with a quite large characteristic time at room temperature (larger than five days' time). Thus, the nanostructured films that have been fabricated in this work is expected to enhance the reliability of RF MEMS capacitive switches.

5. Conclusions

Nanostructured SiN_x films with embedded CNTs have been fabricated with a simple process, in order to incorporate CNTs on the lower SiN_x layer and thus assist the charge drain towards the bottom metal contact. A reference SiN_x material has been also fabricated with the same method (without CNTs), in order to compare the properties of the nanostructured films with the pristine material. Thermally activated discharging mechanisms of utilized films have been investigated with the aid of MIM capacitors, using TSDC assessment and a single-point KP system for temperatures from 300 K to 400 K.

The nanostructured material is found to exhibit lower charging and smaller discharging time, which is attributed to field enhancement from the presence of CNTs. Two major contributing discharging mechanisms are found in TSDC envelope of both nanostructured and reference materials, and each of them exhibited smaller characteristic time at room temperature and smaller charge in the nanostructured films. Moreover, the TSDC revealed that the presence of CNTs in the nanostructured films diminishes a discharging mechanism in the reference material, which has a characteristic time larger than five days' time at room temperature, a value similar to the discharging time constant of the reference film. This is the first time, to the best of our knowledge, that different discharging mechanisms are identified and distinguished, between the reference and the nanostructured SiN_x dielectric film. In addition, the discharging process due to charge displacement in the bulk material is found to be thermally activated and hopping dominates charge transport. Finally, larger mean hopping distance and zero field conductivity is found for nanostructured films, with respect to the reference material, a result that may be attributed to alternation of the percolation path due to field enhancement, arising from the embedded CNTs.

The simplicity of the deposition process of SiN_x films with embedded CNTs and their electrical properties make these nanostructured films quite promising for the fabrication of reliable RF MEMS capacitive switches. Further investigation regarding the effect of CNTs density as well as the dielectric film structure on the electrical behavior of these films is necessary and presently in progress.

Declaration of Competing Interest

The authors declare that they have no known competing financial interests or personal relationships that could have appeared to influence the work reported in this paper.

Acknowledgements

This work has been financed by the European Union and Greek national funds through the Operational Program Competitiveness, Entrepreneurship and Innovation, under the call RESEARCH – CREATE – INNOVATE. (Project code: T1EDK-00329).

References

[1] G.M. Rebeiz, RF MEMS: Theory Design and Technology, John Wiley & Sons, 2003.
[2] C. Bordas, et al., Carbon nanotube based dielectric for enhanced RF MEMS reliability, IEEE MTT-S Int. Microw. Symp. Dig. 2 (2007) 375–378.
[3] M. Koutsoureli, et al., Electrical properties of nanostructured SiN films for MEMS capacitive switches, J. Micromech. Microeng. 27 (1) (2017).
[4] M. Koutsoureli, G. Stavrinidis, D. Birmpiliotis, G. Konstantinidis, G. Papaioannou, Electrical properties of SiNx films with embedded CNTs for MEMS capacitive switches, Microelectron. Reliab. 76–77 (2017) 614–618.
[5] D. Birmpiliotis, G. Stavrinidis, G. Konstantinidis, G. Papaioannou, Temperature accelerated discharging process in SiNx films with embedded CNTs for applications in MEMS switches, Symposium on Design, Test, Integration and Packaging of MEMS/MOEMS, DTIP 2018, 3 2018, pp. 1–6.
[6] G. Papaioannou, L. Michalas, M. Koutsoureli, S. Bansropun, A. Gantis, A. Ziaei, Charging mechanisms in nanostructured dielectrics for MEMS capacitive switches, SiRF 2014–2014 IEEE 14th Topical Meeting on Silicon Monolithic Integrated Circuits in RF Systems, 2014, pp. 98–100.
[7] W.M. Van Spengen, Capacitive RF MEMS switch dielectric charging and reliability: a critical review with recommendations, J. Micromech. Microeng. 22 (7) (2012).
[8] X. Rottenberg, I. De Wolf, B.K.J.C. Nauwelaers, W. De Raedt, H.A.C. Tilmans, Analytical model of the DC actuation of electrostatic MEMS devices with distributed dielectric charging and nonplanar electrodes, J. Microelectromech. Syst. 16 (5) (2007) 1243–1253.
[9] W.S. Bao, S.A. Meguid, Z.H. Zhu, Y. Pan, G.J. Weng, Effect of carbon nanotube geometry upon tunneling assisted electrical network in nanocomposites, J. Appl. Phys. 113 (23) (2013).
[10] L. Michalas, et al., Gold nanorod array structured silicon nitride films for reliable RF MEMS capacitive switches, 2015 IEEE 15th Topical Meeting on Silicon Monolithic Integrated Circuits in RF Systems, SiRF 2015, 2015, pp. 89–91.
[11] D. Birmpiliotis, G. Stavrinidis, M. Koutsoureli, G. Konstantinidis, G. Papaioannou, A. Ziaei, A comparative study of nanostructured silicon-nitride electrical properties for potential application in RF-MEMS capacitive switches, Microelectron. Reliab. (June) (2019) 113360.
[12] G. Papaioannou, M.N. Exarchos, V. Theonas, G. Wang, J. Papapolymerou, Temperature study of the dielectric polarization effects of capacitive RF MEMS switches, IEEE Trans. Microw. Theory Tech. 53 (11) (2005) 3467–3473.
[13] M. Lamhamdi, et al., Voltage and temperature effect on dielectric charging for RF-MEMS capacitive switches reliability investigation, Microelectron. Reliab. 48 (8–9) (2008) 1248–1252.
[14] G. Papaioannou, N. Tavassolian, M. Koutsoureli, E. Papandreou, J. Papapolymerou, Investigation of charging mechanisms in RF-MEMS capacitive switches with silicon nitride: the effect of material stoichiometry, IEEE MTT-S International Microwave Symposium Digest, 0 2009, pp. 1653–1656.
[15] M. Koutsoureli, N. Siannas, G. Papaioannou, Temperature accelerated discharging processes through the bulk of PECVD silicon nitride films for MEMS capacitive switches, Microelectron. Reliab. 76–77 (2017) 631–634.
[16] G. Papaioannou, F. Coccetti, R. Plana, On the modeling of dielectric charging in RF-MEMS capacitive switches, 2010 *10th Top. Meet. Silicon Monolith. Integr. Circuits RF Syst. SiRF* 2010 - *Dig. Pap*, 2010, pp. 108–111.
[17] A. Jain, S. Palit, M.A. Alam, A physics-based predictive modeling framework for dielectric charging and creep in RF MEMS capacitive switches and varactors, J. Microelectromech. Syst. 21 (2) (2012) 420–430.
[18] A.C. Amiaud, A. Leuliet, B. Loiseaux, J.P. Ganne, J. Nagle, Modeling of dielectric charging in capacitive structures, J. Appl. Phys. 118 (17) (2015).
[19] S.M. Sze, Current transport and maximum dielectric strength of silicon nitride films, J. Appl. Phys. 38 (7) (1967) 2951–2956.
[20] R. Ramprasad, Phenomenological theory to model leakage currents in metal-insulator-metal capacitor systems, Phys. Status Solidi Basic Res. 239 (1) (2003) 59–70.
[21] J.G. Simmons, Poole-Frenkel effect and Schottky effect in metal- insulator-metal systems, Phys. Rev. 155 (3) (1967).
[22] M. Koutsoureli, et al., Charging and discharging processes in ALN dielectric films deposited by plasma assisted molecular beam epitaxy, Proceedings of the International Semiconductor Conference, 2 CAS, 2012, pp. 281–284.
[23] N.F. Mott, Conduction in non-crystalline materials, Philos. Mag. 19 (160) (1969) 835–852.
[24] R.M. Hill, Hopping conduction in amorphous solids, Philos. Mag. 24 (192) (1971) 1307–1325.
[25] N. Apsley, H.P. Hughes, Temperature- and field-dependence of hopping conduction in disordered systems, II, Philos. Mag. 31 (6) (1975) 1327–1339.
[26] M. Pollak, I. Riess, A percolation treatment of high-field hopping transport, J. Phys. C Solid State Phys. 9 (12) (1976) 2339–2352.
[27] F.C. Chiu, A review on conduction mechanisms in dielectric films, Adv. Mater. Sci. Eng. 2014 (2014).
[28] M.P. Fateev, Theory of hopping transfer in disordered systems, Phys. Solid State 52 (6) (2010) 1123–1130.
[29] KP Technology Kelvin Probe Manual.pdf, [Online]. Available http://www.kelvinprobe.com/science.php.
[30] J. Vanderschueren, J. Casiot, Thermally stimulated relaxation in solids - field induced thermally stimulated currents, in: P. Braunlich (Ed.), Topics in Applied Physics, Springer Verlag, 1979, pp. 135–219.
[31] M. Koutsoureli, G. Papaioannou, Determination of long time discharge current in microelectromechanical system capacitive switches, Appl. Phys. Lett. 99 (10) (2011).
[32] J.C. Phillips, Stretched exponential relaxation in molecular and electronic glasses, Rep. Prog. Phys. 59 (9) (1996) 1133–1207.
[33] M. Koutsoureli, L. Michalas, G. Papaioannou, Charge collection mechanism in MEMS capacitive switches, International Reliability Physics Symposium (IRPS), 2012, pp. 1–5 (vol. c).
[34] E. Papandreou, M. Lamhamdi, C.M. Skoulikidou, P. Pons, G. Papaioannou, R. Plana, Structure dependent charging process in RF MEMS capacitive switches, Microelectron. Reliab. 47 (9–11) (2007) 1812–1817 SPEC. ISS.

Microelectronics Reliability 114 (2020) 113878

Contents lists available at ScienceDirect

Microelectronics Reliability

journal homepage: www.elsevier.com/locate/microrel

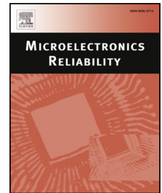

A study of hopping transport during discharging in SiN_x films for MEMS capacitive switches

D. Birmpiliotis[a,*], M. Koutsoureli[a], G. Stavrinidis[b], G. Konstantinidis[b], G. Papaioannou[a]

[a] Condensed Matter Physics Section, University of Athens, GR-15784 Athens, Greece
[b] Institute of Electronic Structures and Lasers (IESL), Foundation for Research and Technology Hellas (FORTH), Heraklion 70013, Greece

ABSTRACT

A more realistic approach of the discharging process in MEMS capacitive switches is presented with the introduction of the effective temperature in order to determine the behavior of the microscopic parameters of hopping conduction, which dominates the process. The use of Kelvin Probe method in MIM capacitors that simulates the discharging process in MEMS switches during up-state revealed that both the increase of temperature and stressing field intensity results the decrease of mean hopping length. This result arises from the simultaneous contribution of the transport energy levels associated with the impact of the stressing field and temperature. Also, a correlation was found experimentally between the stretched exponential decay and the hopping process. The proposed method was also applied in MEMS switches where a similar behavior of the hopping parameters was found, providing evidence that the control of the hopping length to an optimum value can provide fast discharging and low leakage currents, increasing the device lifetime.

1. Introduction

RF-MEMS capacitive switches possess many benefits over both conventional switches such as FETs or PIN diodes and ohmic ones. Their ultra-high linearity, almost zero power consumption, compatibility with silicon technology and their ability to manage signals up to hundreds of GHz, makes them the most prominent candidate to overcome the limitations arising from the use of conventional semiconductor based switches [1]. However, reliability issues, among them the most severe is dielectric charging, hinder their introduction to mass production. During the devices' operation, specifically during actuation, charges are injected and trapped inside the dielectric causing erratic device behavior which in most cases may lead to stiction or shift of pull-in voltage beyond the actuation one resulting the device failure.

In a MEMS capacitive switch, during up-state, the stored charge can only be drained through the bottom electrode. Therefore, the device lifetime is determined by the charging and discharging rates. The dielectric film charging occurs under high electric fields and therefore is a rather fast process if compared to discharging. This has been confirmed from unipolar cycling tests which always lead to stiction as shown in [2,3]. Moreover it has been shown that the number of cycles to the end of life decreases exponentially with increasing the actuation voltage [4].

In order to mitigate the dielectric charging and increase the ON/OFF capacitance ratio several materials have been applied such as SiO_2 [5,6], AlN [7], Al_2O_3 [8], Y_2O_3 [9] and SiN_x [10,11]. The dielectric charging in MIM capacitors (Metal-Insulator-Metal) has been initially assessed with recording the charging/discharging current transients [5] and TSDC (Thermally Stimulated Depolarization Current) spectroscopy [7], which provided information on the charge exchange between the injecting electrodes and the dielectric film. Methods that allowed the monitor of discharge process through the dielectric film were based on using the KPFM (Kelvin Probe Force Microscopy) to monitor the discharge on a MEMS dielectric film [12] or the free surface of a dielectric film [13,14], all affected by lateral charge diffusion. Finally, the Kelvin Probe method has been applied to calculate the discharge current through the dielectric film in MEMS [15] and MIM [16] and both [17]. The later intended the better understanding of the hopping transport in Si-rich silicon nitride and its dependence on material stoichiometry, deviations from homogeneity as well as the impact of extrinsic effects such as humidity.

The abovementioned methods aimed to understand the conduction mechanism/s that would balance the charging rate and lead to a steady state condition corresponding to a minimal shift of C-V characteristic under unipolar stress. Achieving such condition, the shift of pull-in voltage will not exceed the actuation one, the Frenkel-Poole transport mechanism, which requires higher electric fields will have minor contribution during discharge process in the rest position, therefore the charging reliability issue will effectively be mitigated and the charge transport in the up-state rest position will be carried out through low or high field hopping transport.

The majority of presently available studies on the MEMS dielectric

* Corresponding author.
E-mail address: dimbir@phys.uoa.gr (D. Birmpiliotis).

https://doi.org/10.1016/j.microrel.2020.113878
Received 25 May 2020; Received in revised form 17 July 2020; Accepted 22 July 2020
Available online 31 October 2020
0026-2714/ © 2020 Elsevier Ltd. All rights reserved.

film discharge (see above mentioned references and their citations) have adopted a single or multiexponential decay, stretched exponential decay and other macroscopic models [18–21] which effectively simulate the discharging process but did not provide insight and therefore the possibility of material engineering for charging mitigation.

In previous studies including those performed at different temperatures [11] the fact that the electric field plays a role similar to that of temperature [22,23] was not considered. According to [22,23], at high electric fields the temperature has to be replaced by an effective one $T_{eff}(T_{amb},F)$, which is determined by the device temperature and the applied field.

Considering the necessity of suppressing the dielectric charging at early stages, that is the shift of C-V characteristic is still small and where the hopping transport still dominates, the present work aims to provide a better understanding of the discharge including microscopic material parameters such as hopping distance and hopping barrier. The investigation aims to understand the effect of device temperature on these devices in order to provide a tool for the material engineering and the prediction of charging behavior under different conditions targeting the increase of operating lifetime. The assessment includes both MIMs and MEMS capacitive switches, performed at different temperatures and charging levels, allowing the determination of thermally activated mechanisms and the effect of internal electric field after each charging level on material microscopic parameters.

2. Theoretical background

Studying the hopping transport in amorphous semiconductors in the presence of a strong electric field, B. Shklovskii [24] has shown that for finite temperatures and in the absence of electric fields, the hopping transport takes place in the so called transport energy level ε_T, defined as the energy of those sites that a charge carrier visits with highest probability independent of the starting position [25], where the hopping rate maximizes:

$$\varepsilon_T = 3\varepsilon_0\, ln\left[\frac{3\varepsilon_0\left(\frac{4\pi N}{3}\right)^{\frac{1}{3}}\alpha}{2kT_{amb}}\right] \tag{1}$$

In Eq. (1) k is the Boltzmann constant, ε_0 is the band tail width, N the concentration of localized states and T_{amb} the device temperature. The localization length a describes the spatial extent of the wave function localized at a single site and depends on the material lattice properties. The value of a is estimated to 0.77 nm and 0.56 nm for a-Se and PbO [26], 0.5–0.8 Å for Li_xWO_y [27] and 1–2 nm in a-Si [28,29]. In the present work the adopted value of a was 1 nm.

It was also shown that in the presence of a strong electric field at $T = 0$, an analogous energy level (ε_F) arises because of the increase of the electron energy ($\varepsilon = qFr_{ij}$), where F is the electric field intensity, relative to the mobility edge by hopping against the electric field over a distance r_{ij} (Fig. 1a) [30]:

$$\varepsilon_F = 3\varepsilon_0 \ln\left[\frac{3\varepsilon_0 N^{\frac{1}{3}}}{2\gamma qF}\right] \tag{2}$$

where q is the elementary charge and the parameter γ has the value γ ≈ 0.67.

According to these, the combined effect of the electric field during discharging F_i and ambient temperature T_{amb} on the hopping conductivity can be expressed with the introduction of the effective temperature [22]:

$$T_{eff}^2(F_i, T) = T_{amb}^2 + \left(\frac{\gamma\cdot q\cdot F_i\cdot a}{k}\right)^2 \tag{3}$$

Here we should bear in mind that discharging takes place under the presence of T_{eff}, which reaches T_{amb} as $F_i \rightarrow 0$.

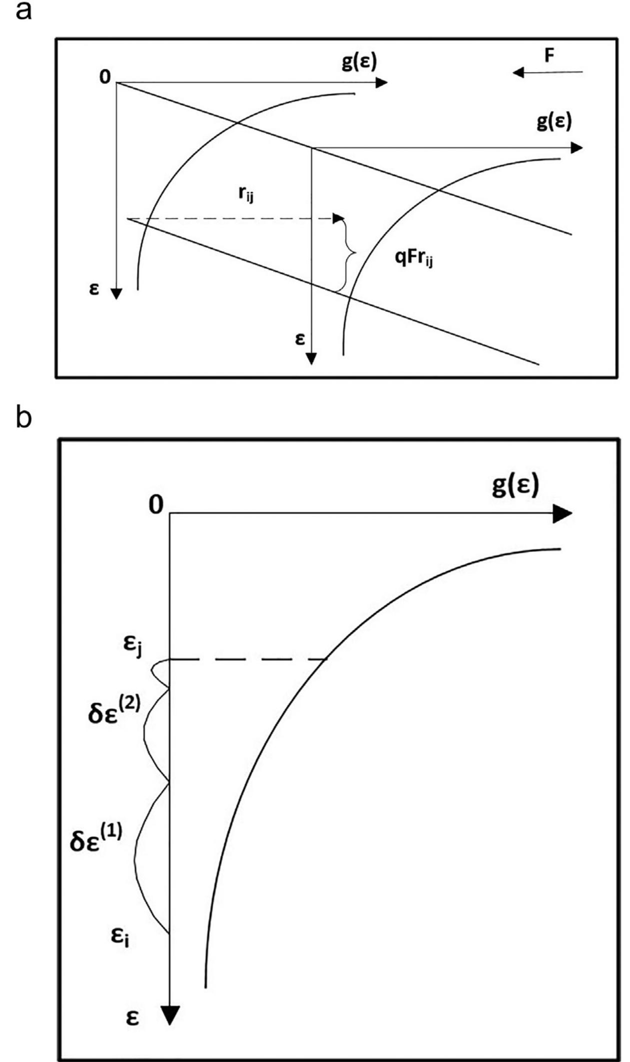

Fig. 1. a) Electron hop against the electric field over the distance r_{ij}, b) The increase of electron energy by $\delta\varepsilon^{(1)}$, $\delta\varepsilon^{(2)}$ etc. with respect to the mobility edge due to successive hops against the field direction.

According to R. M. Hill [31] and M. Pollak et al., [32], the expression of hopping current density including T_{eff} is:

$$J_H = \sigma^*\cdot F_i\cdot exp\left(\frac{q\cdot r_{ij}\cdot F_i}{kT_{eff}}\right) \tag{4}$$

where r_{ij} the mean hopping distance and

$$\sigma^* = \sigma_0\cdot exp\left(-\frac{r_{ij}}{a} - \frac{\Delta E}{kT_{amb}}\right) \tag{5}$$

where σ_0 is the fitting conductivity which depends on the electron-phonon coupling strength, the phonon density of states and other properties of the material [33] and ΔE is the mean energy separation between the hopping sites expressing the classical hopping of a carrier over the potential barrier separating two energetically favorable sites, i.e. in a double well potential [34] or the hopping barrier height for DC conduction [35].

In the case of MIM capacitor the electric field is determined from the top electrode potential U_s and the dielectric film thickness d_ε ($F_i = U_s/d_\varepsilon$), thus the current density can be expressed as [36]:

$$J(t) = -\frac{\varepsilon_0\cdot\varepsilon_r}{d_\varepsilon}\cdot\frac{dU_s(t)}{dt} \tag{6}$$

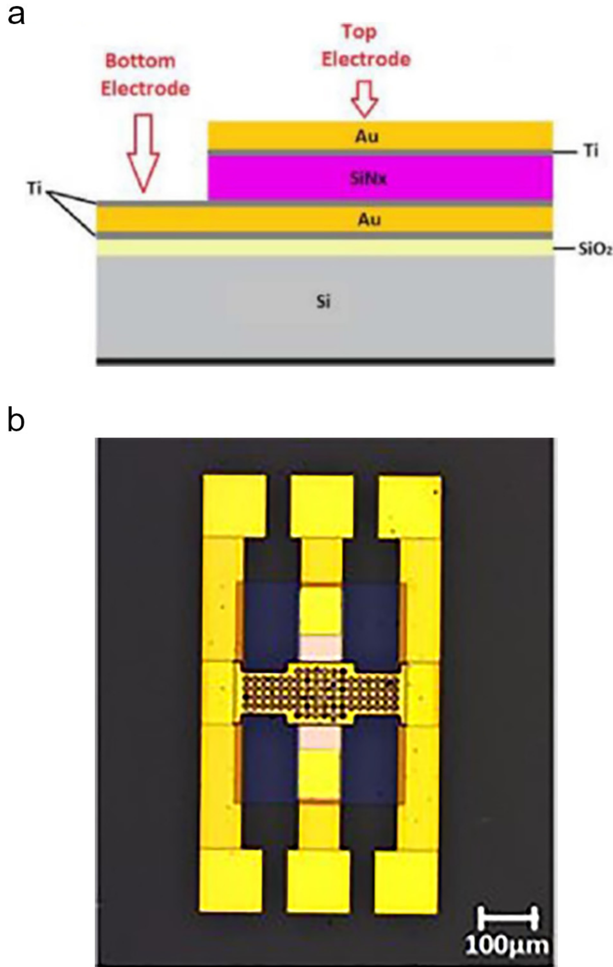

Fig. 2. Schematic of the utilized a) MIM capacitors and b) MEMS capacitive switches.

Assuming that hopping dominates the discharging process [17,37] $J(t) = J_H$, and combining Eqs. (4) and (6) yields:

$$t = t_0 - \frac{\varepsilon_0 \varepsilon_r}{\sigma^*} \int_{U_{s,0}}^{U_s(t)} \frac{dU_s}{U_s \exp\left(\frac{q \cdot r_{ij}}{kT_{eff} d_\varepsilon} U_s\right)} \tag{7}$$

which associates the discharging time with the surface potential. In the case of MEMS capacitive switches the current density during discharging can be evaluated with the substitution $U_s(t) = V_{min}(t)$ in Eq. (6), where V_{min} is the voltage value that corresponds to minimum capacitance, assuming a small capacitance variance [15,38,39]. Considering the fact that during discharging T_{eff} is time dependent, r_{ij} is treated as a constant fitting parameter.

3. Experimental details

The MIM capacitors used in the present work fabricated with standard photolithographic process where the circular top electrode had a diameter of 2 mm (Fig. 2). Both electrodes where symmetric Ti/Au layers in order to minimize the impact of the contact interface asymmetry. The SiNx film thickness was 200 nm and deposited with PECVD method at substrate temperature of 250 °C. The film stoichiometry was measured by X-ray Photoelectron Spectroscopy (XPS) and was found to be 0.57, indicating a Si-Rich film.

The discharge process on MIM capacitors was monitored with the aid of Kelvin Probe method. The Kelvin Probe is a non-contact, non-destructive vibrating capacitor device used to measure contact potential difference between a conducting specimen and a vibrating probe tip, which is placed near the surface of interest [40]. The surface potential (U_s) of the utilized devices is thus directly measured during discharge, while the device is not in contact with the measuring system. A polarization field with intensities of 250 to 1000 kV/cm with steps of 250 kV/cm has been applied for 15 min in ambient, while in order to study the impact of the temperature on the discharging process each experiment was performed in the range of 300 K–340 K with steps of 10 K. The following discharging process has been assessed by measuring the decay of surface potential (U_s) for a time period of about 10^4s. In all measurements, the polarization bias has been applied on the top metal electrode.

For the MEMS switches, the dielectric film was grown on top of a Cr/Au bottom metal electrode. The SiNx film thickness was 200 nm and the deposition was performed with high frequency (13.56 MHz) PECVD method at substrate temperature of 300 °C. The membrane is an evaporated Cr/Au layer and in the unactuated position, it is suspended about 1 µm above the dielectric. The pull-in voltage of the switches has been found to be about Vpi ≈ 35 V. MEMS devices were stressed at 40 V for 20 min in the temperature range 300 K–380 K in steps of 20 K, while the discharge process was assessed by monitoring the bias for capacitance minimum (V_{min}) of up-state capacitance-voltage (C-V) characteristics with a Boonton 72B capacitance meter. The required bias was applied to the transmission line with 487 Keithley voltage source-picoampere meter. The bias for up state capacitance minimum was determined by fitting a parabola to the experimental data, assuming small capacitance variance. All measurements on MEMS switches have been performed in a cryostat, under vacuum, with prior 2 h annealing at 160 °C, in order to avoid any spurious effects due to humidity.

4. Results and discussion

4.1. MIM capacitors-the impact of stressing field level

As already mentioned through the Kelvin Probe method the stored charge can only be drained from the bottom electrode, thus the discharging current provides information about the charge kinetics and the associated transport mechanism. For each stressing field and at each temperature the potential decay was fitted with Eq. (7); indicatively in Fig. 3 are shown the fitting results after stressing with 1MV/cm. In this high stressing field level the charge redistribution through the Frenkel-Poole mechanism cannot be disregarded. However, discharging initiates under the presence of low internal electric field intensities, approximately 500 kV/cm, thus it is expected that discharging will be dominated by the high field hopping conduction.

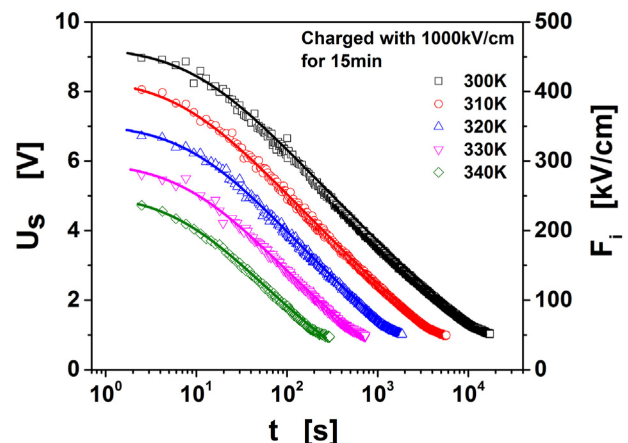

Fig. 3. The potential decay at each temperature after isochronal charging with 1MV/cm.

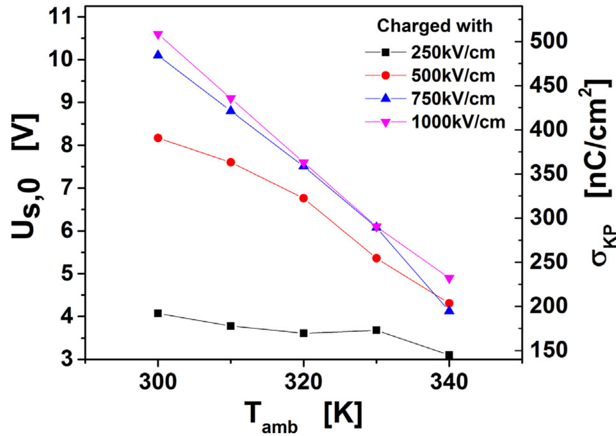

Fig. 4. Plot of $U_{s,\ t=0}$ vs charging temperature for the applied stressing fields and the calculated surface charge density.

The dependence of MIM capacitor top electrode potential ($U_{s,\ t=0}$) after isochronal charging at different temperatures for all the applied stressing fields is shown in Fig. 4. In all cases, the starting potential and the calculated stored charge density σ_{KP} drops with increasing temperature, a behavior that is more intense for larger charging fields.

Applying Eq. (7) to the experimental decays at each device temperature and stressing field intensity allowed the calculation of the mean hopping length, which decreases with the increase of stressing field (Fig. 5) and/or temperature (Fig. 6).

This behavior can be interpreted by the following: Considering only the impact of stressing field intensity its increase results the increase of mobility band bending and the consequent charge trapping giving rise to the initial potential. Also, during charging the charge injection takes place through trap assisted tunneling (TAT), which is strongly field and temperature dependent, and is partly compensated by the charge redistribution through Frenkel-Poole or hopping mechanism. The charge redistribution is determined by the stressing field which also affects the carrier occupancy in band tails and therefore r_{ij}. Following Eq. (2), during discharging at a specific F_{stress} and T, the continuous decrease of Us is a result of the movement of the level ε_F, where hopping rate maximizes, towards Fermi level. This shift of ε_F exposes areas of fewer defects resulting larger and fewer hops, since the hopping rate is proportional to the effective defect density ($N_{eff} = 1/r_{ij}^3$). Here it must be emphasized that the calculated value of N_{eff} corresponds to the effective defects participating in the process rather than the total intrinsic defect concentration which depends on material properties [24]. The gradual increase of stressing field intensity which also increases $U_{s,\ t=0}$ (Fig. 4)

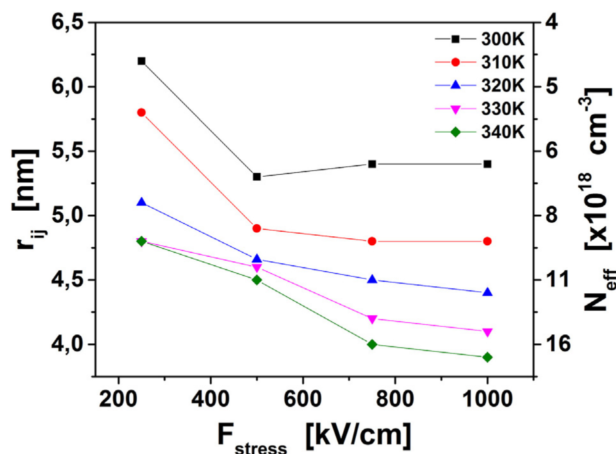

Fig. 5. Plot of the calculated r_{ij} vs stressing field intensity.

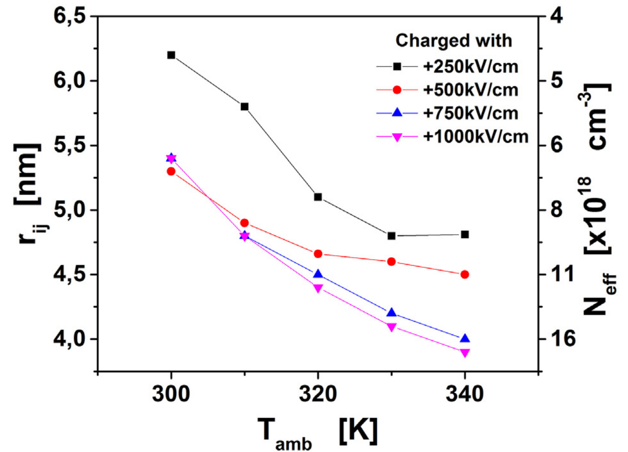

Fig. 6. The mean hopping length as function of the ambient temperature at each applied electric field intensity.

shifts ε_F to more shallow states, where more and shorter hops are favored, leading to increased conductivity (Fig. 5).

4.2. MIM capacitors-the impact of device temperature

In the other hand, the impact of device temperature on the discharging process (Fig. 6), is attributed to the fact that an analogous energy level (ε_T) arises, the so called transport energy (Eq. (1)) [22], which gradually moves with increasing T_{amb} from the Fermi level towards mobility band edge. Since in amorphous SiNx the density of states in the band tails increases exponentially towards mobility band edge, the hopping distance will decrease. This also justifies the increase of calculated apparent effective density of states, while the decay of top electrode potential will make its contribution less effective to T_{eff} (Eq. (3)).

The zero-field conductivity was found to be thermally activated, where the corresponding Arrhenius plot is presented in Fig. 7. The calculated average activation energy was found to be 0.97 eV ± 0.04 eV. This large activation energy does not correspond to energy difference between states in the band tails but rather to the parabolic barrier separating the states.

Discharging process is faster at short times followed by slower process as time increases. Considering the fact that the decrease of electric field results also the decrease of band bending moving towards equilibrium so that the apparent density of states decreases. This gives rise to the hierarchical scheme of the discharging process where short

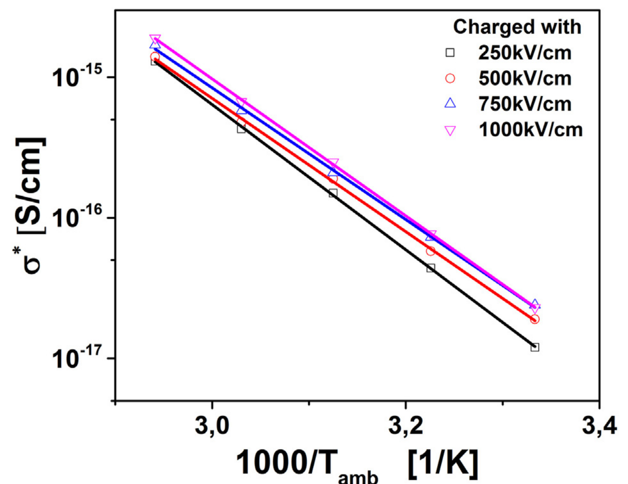

Fig. 7. Arrhenius plot of zero field conductivity at each stressing field intensity.

hops are followed by larger hops (Fig. 1b).

4.3. Relation to stretched exponential decay

It is widely accepted that the stretched exponential function, known as the Kohlrausch-Williams-Watts (KWW) law, can describe many relaxation phenomena in complex condensed matter systems including glasses, polymers, amorphous silicon and other systems. In the case of the top electrode potential decay due to charge transport through the bulk the function is given by:

$$U_s(t) = U_{s,0}\cdot exp\left[-\left(\frac{t}{\tau}\right)^{\beta}\right] \tag{8}$$

where β is the stretching index ranging from 0 to 1 and τ the time constant of the relaxation process. The parameters β and τ depend on the material and can be a function of external variables such as temperature.

Several efforts have been paid in the search of microscopic models responsible for generating the stretched exponential law, including the Förster direct-transfer mechanism [41] of charge relaxation via parallel channels, the serial hierarchically constrained dynamics model [42] and the defect diffusion model of Shlesinger and Montroll [43]. Sturman et al. [44] derived a geometric approach of a hopping model where the stretched exponential law originates from the geometric features of a random distribution of transport and trapping sites in the 3D space. Also, they found that the value of stretching index β is determined by the localization radius of hopping electrons, however an analytical expression of the dependence of β on r_{ij} has not been derived. In addition, it was found that the stretching index increases with the increase of trap density and decreases with the increase of hopping length. Fig. 8 shows the experimental dependence of the r_{ij} calculated with Eq. (7) and the stretching index β which was determined by applying Eq. (8) for each stressing field and at each temperature. This leads us to the conclusion that the extracted fitting parameters with Eq. (8) and the extracted values of r_{ij} can be correlated experimentally, providing results directly related to the material properties.

4.4. MEMS capacitive switches

The proposed model has been further applied to MEMS capacitive switches, where the behavior of the calculated r_{ij} is presented in Fig. 9. The increase of temperature results the decrease of r_{ij} in a similar way as MIM capacitors. The obtained differences in the calculated values arise from the fact that the dielectrics used in MIMs and MEMS switches were

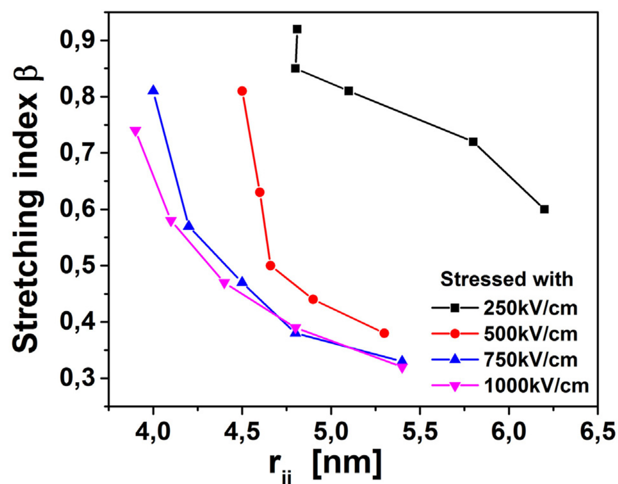

Fig. 8. The dependence of stretching index β with the calculated hopping length for each applied electric field intensity and device temperature.

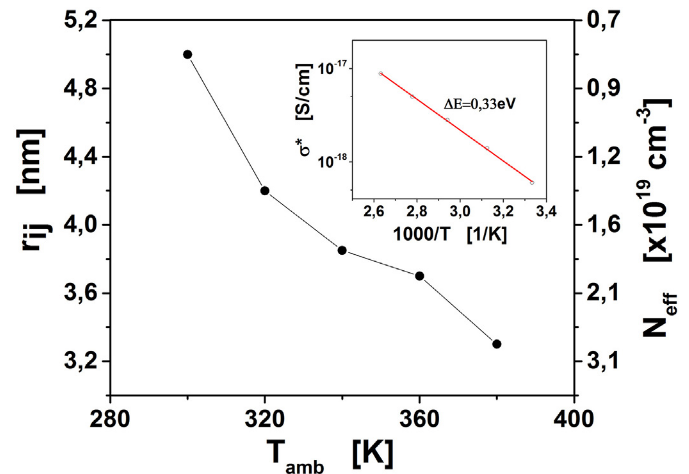

Fig. 9. The mean hopping length vs T_{amb} calculated with the proposed model for MEMS capacitive switches. Inset: Arrhenius plot of σ^{*}.

fabricated with different conditions, resulting to different material stoichiometry, and affecting the material bandgap as well as the defect concentration. The zero-field conductivity was also found to be thermally activated with an activation energy of 0.33 ± 0.01 eV. Considering the impact of the stressing field and device temperature on the discharging procedure through the dielectric bulk during up-state in MEMS, the ability to control the parameters ε_F and ε_T is essential. The knowledge of the position of these levels would allow one to estimate at which position within the density of states, its modification by adding dopants or impurities through the fabrication process has the greatest effect on the transport characteristics of the material.

5. Conclusions

A more realistic approach of the discharging process in MEMS capacitive switches is presented with the introduction of the effective temperature in order to assess the behavior of the microscopic parameters of hopping conduction, which dominates the process. The use of Kelvin Probe method in MIM capacitors that simulates the discharging process in MEMS switches during up-state revealed that both the increase of temperature and stressing field intensity results to the decrease of mean hopping length. This result arises from the simultaneous contributions of the movement of the energy levels ε_F, ε_T and the exponential increase of the density of states in the band tail towards mobility edge. Moreover, it was found experimentally that the extracted parameters of the macroscopic stretched exponential decay can be correlated with the parameters of the microscopic hopping process. Also, it was found that the potential barrier between the hopping sites is independent of stressing field intensity while the calculated activation energy corresponds to a parabolic potential barrier.

The proposed method was also applied in MEMS switches where a similar behavior of the hopping parameters was found. This provides evidence that the proposed tool can be used for material optimization, where the control of the hopping length may lead to the adjustment of its value in order to provide fast discharge and low leakage currents, increasing the device lifetime.

CRediT authorship contribution statement

D. Birmpiliotis: Investigation, Data curation, Formal analysis, Software, Visualization, Writing - review & editing. **M. Koutsoureli:** Data curation, Validation, Writing - review & editing. **G. Stavrinidis:** Resources. **G. Konstantinidis:** Funding acquisition, Resources. **G. Papaioannou:** Conceptualization, Methodology, Validation, Supervision, Project administration, Resources, Writing - review &

editing.

Declaration of competing interest

The authors declare that they have no known competing financial interests or personal relationships that could have appeared to influence the work reported in this paper.

Acknowledgements

This work is partially co-financed by Greece and the European Union (European Social Fund-ESF) through the Operational Programme "Human Resources Development, Education and Lifelong Learning" in the context of the project "Strengthening Human Resources Research Potential via Doctorate Research" (MIS-5000432), implemented by the State Scholarships Foundation (IKY). Also has been co-financed by the European Union and Greek National Funds through the Operational Program Competitiveness, Entrepreneurship and Innovation, under the call RESEARCH – CREATE – INNOVATE (Project code: T1EDK-00329).

References

[1] G.M. Rebeiz, RF MEMS: Theory, Design, and Technology, J. Willey and Sons, Hoboken, 2004.
[2] W.M. van Spengen, R. Puers, R. Mertens, I. De Wolf, A low frequency electrical test set-up for the reliability assessment of capacitive RF MEMS switches, J. Micromech. Microeng. 13 (5) (2003) 604.
[3] W.M. van Spengen, Capacitive RF MEMS switch dielectric charging and reliability: a critical review with recommendations, J. Micromech. Microeng. 22 (7) (2012).
[4] C. Goldsmith, et al., Lifetime characterization of capacitive RF MEMS switches, Microwave Symposium Digest, 2001 IEEE MTT-S International, vol. 1, IEEE, 2001, pp. 227–230.
[5] Y. Xiaobin, J.C.M. Hwang, D. Forehand, C.L. Goldsmith, Modeling and characterization of dielectric-charging effects in RF MEMS capacitive switches, IEEE MTT-S International Microwave Symposium Digest, 2005, 2005 (pp. 4 pp.-756).
[6] G. Papaioannou, F. Giacomozzi, E. Papandreou, B. Margesin, Floating electrode microelectromechanical system capacitive switches: a different actuation mechanism, Appl. Phys. Lett. 99 (7) (2011) 073501 2011/08/15.
[7] E. Papandreou, G. Papaioannou, T. Lisec, A correlation of capacitive RF-MEMS reliability to AlN dielectric film spontaneous polarization, Int. J. Microw. Wirel. Technol. 1 (1) (2009) 43–47.
[8] A. Crunteanu, F. Dumas-Bouchiat, C. Champeaux, A. Catherinot, P. Blondy, Electrical conduction mechanisms of metal nanoclusters embedded in an amorphous Al2O3 matrix, Thin Solid Films 515 (16) (2007) 6324–6327.
[9] D. Birmpiliotis, M. Koutsoureli, J. Kohylas, G. Papaioannou, A. Ziaei, Charging mechanisms in Y2O3 dielectric films for MEMS capacitive switches, Microelectron. Reliab. 88-90 (2018) 840–845 2018/09/01/.
[10] G. Papaioannou, M.-N. Exarchos, V. Theonas, G. Wang, J. Papapolymerou, Temperature study of the dielectric polarization effects of capacitive RF MEMS switches, IEEE Trans. Microw. Theory Tech. 53 (11) (2005) 3467–3473.
[11] M. Koutsoureli, N. Siannas, G. Papaioannou, Temperature accelerated discharging processes through the bulk of PECVD silicon nitride films for MEMS capacitive switches, Microelectron. Reliab. 76-77 (2017) 631–634.
[12] R. Herfst, P. Steeneken, J. Schmitz, A. Mank, M. Van Gils, Kelvin probe study of laterally inhomogeneous dielectric charging and charge diffusion in RF MEMS capacitive switches, 2008 IEEE International Reliability Physics Symposium, IEEE, 2008, pp. 492–495.
[13] U. Zaghloul, G.J. Papaioannou, F. Coccetti, P. Pons, R. Plana, A systematic reliability investigation of the dielectric charging process in electrostatically actuated MEMS based on Kelvin probe force microscopy, J. Micromech. Microeng. 20 (6) (2010).
[14] C. Villeneuve-Faure, K. Makasheva, L. Boudou, G. Teyssedre, Space charge at Nanoscale: Probing injection and dynamic phenomena under dark/light configurations by using KPFM and C-AFM, Electrical Atomic Force Microscopy for Nanoelectronics, Springer, 2019, pp. 267–301.
[15] M. Koutsoureli, G. Papaioannou, Determination of long time discharge current in microelectromechanical system capacitive switches, Appl. Phys. Lett. 99 (10) (2011) 103503 2011/09/05.
[16] M. Koutsoureli, L. Michalas, A. Gantis, G. Papaioannou, A study of deposition conditions on charging properties of PECVD silicon nitride films for MEMS capacitive switches, Microelectron. Reliab. 54 (9–10) (2014) 2159–2163.
[17] D. Birmpiliotis, G. Stavrinidis, M. Koutsoureli, G. Konstantinidis, G. Papaioannou, On the discharge transport mechanisms through the dielectric film in MEMS capacitive switches, J. Microelectromech. Syst. 29 (2) (2020) 202–213.
[18] R.W. Herfst, P.G. Steeneken, J. Schmitz, Time and voltage dependence of dielectric charging in RF MEMS capacitive switches, 2007 IEEE International Reliability Physics Symposium Proceedings. 45th Annual, 2007, pp. 417–421.
[19] D. Mardivirin, A. Pothier, M. El Khatib, A. Crunteanu, O. Vendier, P. Blondy, Reliability of dielectric less electrostatic actuators in RF-MEMS ohmic switches, 2008 European Microwave Integrated Circuit Conference, IEEE, 2008, pp. 490–493.
[20] D. Andrade-Miceli, P. Giounalis, S. Gorreta, J. Pons-Nin, M. Dominguez-Pumar, E. Blokhina, Circuit considerations and design for MEMS capacitance measurements, 2016 12th Conference on Ph. D. Research in Microelectronics and Electronics (PRIME), IEEE, 2016, pp. 1–4.
[21] P. Giounanlis, S. Gorreta, M. Dominguez-Pumar, J. Pons-Nin, O. Feely, E. Blokhina, $\Sigma\Delta$ effects and charge locking in capacitive MEMS under dielectric charge control, IEEE Trans. Circuits Syst. II Express Briefs 64 (2) (2016) 206–210.
[22] S. Marianer, B.I. Shklovskii, Effective temperature of hopping electrons in a strong electric field, Phys. Rev. B 46 (20) (1992) 13100.
[23] B. Cleve, B. Hartenstein, S.D. Baranovskii, M. Scheidler, P. Thomas, H. Baessler, High-field hopping transport in band tails of disordered semiconductors, Phys. Rev. B 51 (23) (1995) 16705–16713 06/15/.
[24] B. Shklovskii, Hopping conduction in semiconductors subjected to a strong electric field, Sov. Phys. Semicond. 6 (12) (1973) 1964–1967.
[25] B. Hartenstein, H. Bässler, Transport energy for hopping in a Gaussian density of states distribution, J. Non-Cryst. Solids 190 (1) (1995) 112–116 1995/10/01/.
[26] A. Nenashev, et al., Field-enhanced mobility in the multiple-trapping regime, Phys. Rev. B 98 (3) (2018) 035201.
[27] G.A. Niklasson, A. Norling, L. Berggren, Charge transport between localized states in lithium-intercalated amorphous tungsten oxide, J. Non-Cryst. Solids 353 (47) (2007) 4376–4379 2007/12/01/.
[28] M. Pollak, B. Shklovskii, Hopping Transport in Solids (Modern Problems in Condensed Matter Sciences), (1991).
[29] S.D. Baranovskii, O. Rubel, P. Thomas, Theoretical description of hopping transport in disordered materials, Thin Solid Films 487 (1–2) (2005) 2–7.
[30] B. Shklovskii, E. Levin, H. Fritzsche, S. Baranovskii, Transport, Correlation and Structural Defects, World Scientific, Singapore, 1990.
[31] R.M. Hill, Hopping conduction in amorphous solids, Philos. Mag. 24 (192) (1971) 1307–1325.
[32] M. Pollak, I. Riess, A percolation treatment of high-field hopping transport, J. Phys. C Solid State Phys. 9 (12) (1976) 2339.
[33] V. Ambegaokar, B.I. Halperin, J.S. Langer, Hopping conductivity in disordered systems, Phys. Rev. B 4 (8) (1971) 2612–2620.
[34] S. Elliott, Ac conduction in amorphous chalcogenide and pnictide semiconductors, Adv. Phys. 36 (2) (1987) 135–217.
[35] W.v. Meyer, H. Neldel, Relation between the energy constant and the quantity constant in the conductivity–temperature formula of oxide semiconductors, Z. Tech. Phys. 18 (12) (1937) 588–593.
[36] M. Koutsoureli, L. Michalas, G. Papaioannou, The effect of temperature on dielectric charging of capacitive MEMS, Reliability Physics Symposium (IRPS), 2011 IEEE International, IEEE, 2011pp. 3D. 4.1-3D. 4.7.
[37] L. Michalas, et al., Electrical characterization of undoped diamond films for RF MEMS application, 2013 IEEE International Reliability Physics Symposium (IRPS), 2013 (pp. 6B.3.1-6B.3.7).
[38] M. Koutsoureli, L. Michalas, G. Papaioannou, Charge collection mechanism in MEMS capacitive switches, 2012 IEEE International Reliability Physics Symposium (IRPS), 2012 (pp. ME.2.1-ME.2.5).
[39] M. Koutsoureli, D. Birmpiliotis, L. Michalas, G. Papaioannou, An in depth analysis of pull-up capacitance-voltage characteristic for dielectric charging assessment of MEMS capacitive switches, Microelectron. Reliab. 64 (2016) 688–692.
[40] Kelvin probe information site, Available http://www.kelvinprobe.info/.
[41] T. Förster, Experimental and Theoretical Investigation of the Intermolecular Transfer of Electronic Excitation Energy, (1949).
[42] R.G. Palmer, D.L. Stein, E. Abrahams, P.W. Anderson, Models of hierarchically constrained dynamics for glassy relaxation, Phys. Rev. Lett. 53 (10) (1984) 958–961 09/03/.
[43] M.F. Shlesinger, E.W. Montroll, On the Williams—Watts function of dielectric relaxation, Proc. Natl. Acad. Sci. 81 (4) (1984) 1280–1283.
[44] B. Sturman, E. Podivilov, M. Gorkunov, Origin of stretched exponential relaxation for hopping-transport models, Phys. Rev. Lett. 91 (17) (Oct 24 2003) 176602.

Microelectronics Reliability 138 (2022) 114649

Contents lists available at ScienceDirect

Microelectronics Reliability

journal homepage: www.elsevier.com/locate/microrel

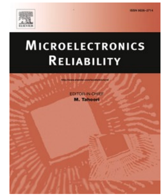

Impact of dielectric film thickness on field emission in MEMS capacitive switches

J. Theocharis *, S. Gardelis, G. Papaioannou

Condensed Matter Physics Section, Physics Department, National and Kapodistrian University of Athens (NKUA), Panepistimiopolis Zografos, 15784 Athens, Greece

ARTICLE INFO

Keywords:
MEMS
Dielectrics
Field emission
Controlled environment
Electrical characterization

ABSTRACT

This study presents experimental evidence of field emission in MEMS capacitive switches. Devices with dielectric layers of silicon nitride of different thicknesses between 50 and 200 nm were investigated by current-voltage (I-V) measurements. These measurements were performed at room temperature and under a controlled atmosphere pressure of 3×10^{-2} mbar at bias levels below breakdown and corresponding electric fields encountered in MEMS capacitive switches during pull-in (1-2 $\times$ 10^6 V/cm). Field emission although was not always clearly observed, it occurred in all devices and clearly manifested at electric fields larger than 10^6 V/cm.

1. Introduction

The electrical properties of dielectric film used in MEMS capacitive switches have been intensively investigated during the last decades because the charging effect determines the device lifetime. The mechanisms responsible for dielectric charging are induced charging arising from free intrinsic charges displacement and dipole orientation [1] and charge injection through contacting electrodes during pull-in or both [2]. A mechanism that has contributed to dielectric charging is the field emission from non-contacting electrodes, specifically from the moving armature. The presence and measurement of field emission current has been reported in [3] and the contribution to dielectric charging compared to conventional devices in [4] both in floating electrode capacitive MEMS.

The conventional capacitive switches have rough electrodes that reduce the maximum capacitance [5] and may create voids. The presence of voids leads to non-uniform capacitance per unit area and surface charge density the modelling of which required detailed approach for each case [6]. Kelvin probe study of surface potential has revealed non uniform charge distribution but of the same polarity [7] that indicated that charging arises from both injected charges through contacting areas and field emission injected charges in the voids.

Presently, in conventional MEMS capacitive switches the identification of each contribution has not been done because the measured current may arise partially from charge transport through the dielectric film and partially from cascade charge transport through field emission followed by transport through the dielectric film.

The present work aims to monitor the field emission in MEMS capacitors without floating electrode. Structures with rigid bridge and different dielectric film thickness are employed. The flowing current through the air gap and dielectric film is measured. The dependence of field emission current on the dielectric film is presented.

2. Background knowledge

2.1. Field emission

Fowler–Nordheim theory describes the emission of electrons from a metal due to very high electric field. This emission process takes place through sharp asperity paths. There the electric field can be locally enhanced by several orders of magnitude, this depending on the asperity shape. The typical signature of this conduction mechanism is the exponential dependence of current on applied bias above a threshold voltage determined by the asperity height and shape. In terms of measured current (I) versus applied bias (V) the Fowler–Nordheim equation is expressed as [8,9]:

$$I_{FN} = \frac{\alpha A V^2}{\Phi t^2(y) d^2} \bullet exp\left(-\frac{B\Phi^{3/2}\nu(y)d}{\beta V}\right)$$
$$A = 6.2 \times 10^{-6} \quad A/eV$$
$$B = 6.85 \times 10^7 \quad V/cm/eV^{3/2} \tag{1}$$

where I_{FN} is the field emission current, α is the effective emitting area, Φ

* Corresponding author.
E-mail address: jtheocharis@phys.uoa.gr (J. Theocharis).

https://doi.org/10.1016/j.microrel.2022.114649
Received 5 June 2022; Received in revised form 13 July 2022; Accepted 14 July 2022
Available online 25 September 2022
0026-2714/© 2022 Elsevier Ltd. All rights reserved.

is the work function, d the gap width, β is the field enhancement factor and A and B are Fowler-Nordheim constants given by:

$$\nu(y) \approx 0.95 - y^2$$

$$t^2(y) \approx 1.1$$

where $y \approx 3.79 \times 10^{-4} \bullet \frac{\sqrt{\beta(V/d)}}{\Phi}$ is a function of the electric field, work function of the metal and the field enhancement factor.

2.2. Emission through barrier

The field emission trough thin dielectric film covering the cathode of electron emitter has received significant attention [10–14]. In MEMS capacitive switches the actuation bias polarity will determine which electrode will play the role of cathode for the field emission process. This leads to two configurations where the "transmission line" will be (i) the cathode when a negative bias is applied with respect to the "bridge" or (ii) the anode when a positive bias will be applied with respect to the "bridge". In the first case the electrons are emitted through a dielectric film. Then the energy diagram for field emission from metal surfaces coated with a dielectric, according to Ref. [14] is presented in Fig. 1.

In all cases the applied bias will be divided in the voltage across the dielectric film (V_d) leading to charge transport and the voltage that will generate the field emission process (V_{FE}). On the other hand, the measured current must be

$$J_{meas} = q\int_0^\infty D(\varepsilon)N(\varepsilon)d\varepsilon \tag{2}$$

and

$$I_{meas} = I_d = I_{FE} \tag{3}$$

where D is the electron transmission probability, N is the number of electrons impinging normal to the metal surface across unit area per unit time [13]. The present work is focused on the case of field emission from the transmission line through the dielectric film towards the device bridge the anode, which is clearly represented in Fig. 1.

3. Device fabrication and experimental procedure

Fig. 2b shows the SEM image of typical dielectric less MEMS device. The fabrication details are the same, except for dielectric film deposition, as the ones outlined in [15]. The fixed–fixed beam is a thick (>6 μm) electroplated Au layer. The beam is made so thick to suffer a negligible deflection when biased against its Au actuation pad underneath it. The gap between the bridge and the coplanar waveguide is 1.5 μm.

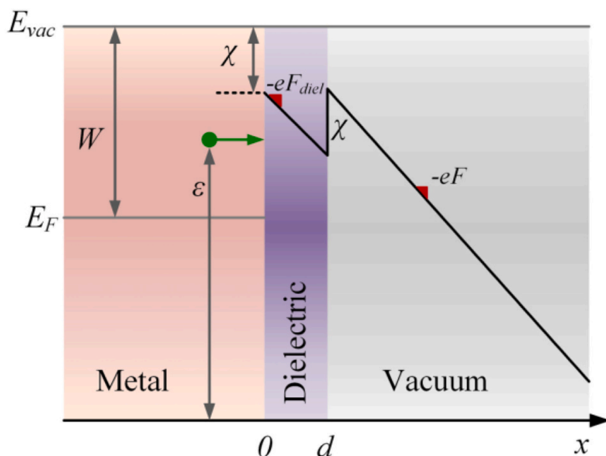

Fig. 1. Energy diagram for field emission from a metal covered with dielectric field based on Ref. [14].

The MEMS capacitors bottom electrode was covered with PECVD Si-rich SiN dielectric film of thickness of 50 nm, 100 nm and 200 nm. The field emission current through the MEMS device was measured with a Keithley 6487 picoammeter, which provided the required bias. Voltages in the range of 0–250 V ere applied to MEMS capacitor through a resistor of $R = 10^9$ Ohm (Fig. 2b) placed in series with the MEMS device to prevent uncontrolled burnout thus allowing the monitoring of field emission current. All measurements were performed at room temperature in a Biorad cryostat under a controlled atmosphere pressure of 3×10^{-2} mbar. In all experiments the applied electric fields did not exceed breakdown hence, corresponding electric fields encountered in MEMS capacitive switches during pull-in (1-2 × 10^6 V/cm). Finally, capacitance-voltage tests were performed with the aid of a Boonton 72 capacitance meter which provided a resolution of 0.5 fF, to test if any bridge is bending.

4. Results and discussion

The thickness of dielectric film (~200 nm) used in MEMS capacitive switches is larger than those reported in [14]. Thus, tunnelling cannot be expected through the dielectric film. To investigate the field emission in such films (Si-rich) SiN films were deposited with progressive increasing thickness of 50 nm, 100 nm and 200 nm and we investigated each case separately.

4.1. The 50 nm dielectric film

The current-voltage (I-V) characteristic, up to breakdown threshold, of a MEMS capacitor with dielectric film of 50 nm is presented in Fig. 3a and the corresponding Fowler-Nordheim plot in the expected field emission regime in Fig. 3b. As already mentioned, the I-V characteristic has been obtained up to the onset of breakdown to avoid major damage to dielectric film.

Analysis of the I-V characteristic reveals that for electric fields above 10^6 V/cm the field emission dominates the flowing current. The straight lines in Fig. 3b show the Fowler-Nordheim fit with the corresponding field enhancement factors. At lower electric fields, down to about 5×10^5 V/cm, the field emission process is still present although the field enhancement factor is about 336 while at higher electric fields the field emission arises from asperities with field enhancement factor of about 99. Here it must be pointed out that the calculated values of the field enhancements factors correspond to the effective ones since field emission must originate from several asperities at the surface of the cathode.

4.2. The 100 nm dielectric film

The current density-electric field (J-E) characteristic, up to breakdown threshold, of a MEMS capacitor with dielectric film of 100 nm is presented in Fig. 4a. The expected field emission region was determined with the aid of Fowler-Nordheim plot and appeared at higher electric fields, Fig. 4a, than those observed in MEMS capacitors with 50 nm dielectric film. This must be attributed to a smoother metallic surface on cathode.

In Fig. 4b the FN plot indicates that before the observed breakdown that usually leads to electrodes damage it appears a sharp peak in the J-E characteristic. The FN plot of this peak shows that it also arises from field emission (Fig. 4b) and the sharp disappearance must be attribute to asperity burning. Finally, the J-E part below field emission region is almost linear and could be attributed to surface leakage since is observed in other devices, i.e., the 200 nm dielectric film ones.

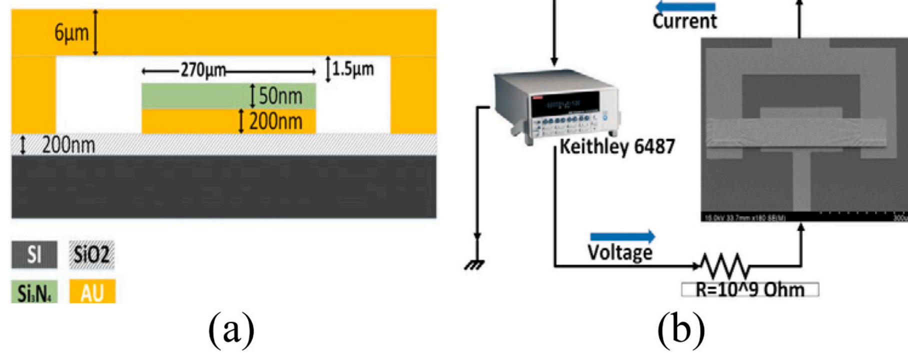

Fig. 2. (a) MEMS device and (b) the I-V assessment setup.

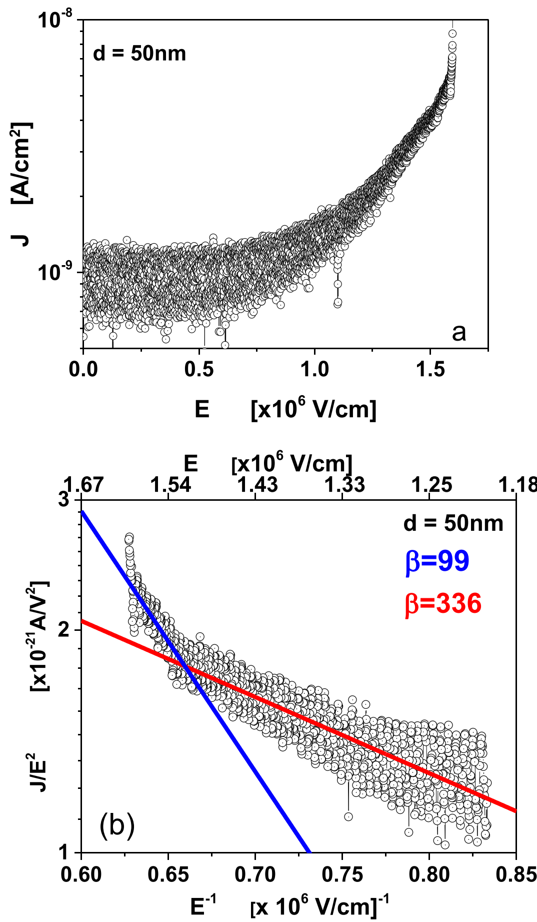

Fig. 3. (a) the I-V characteristic and (b) the Fowler-Nordheim plot.

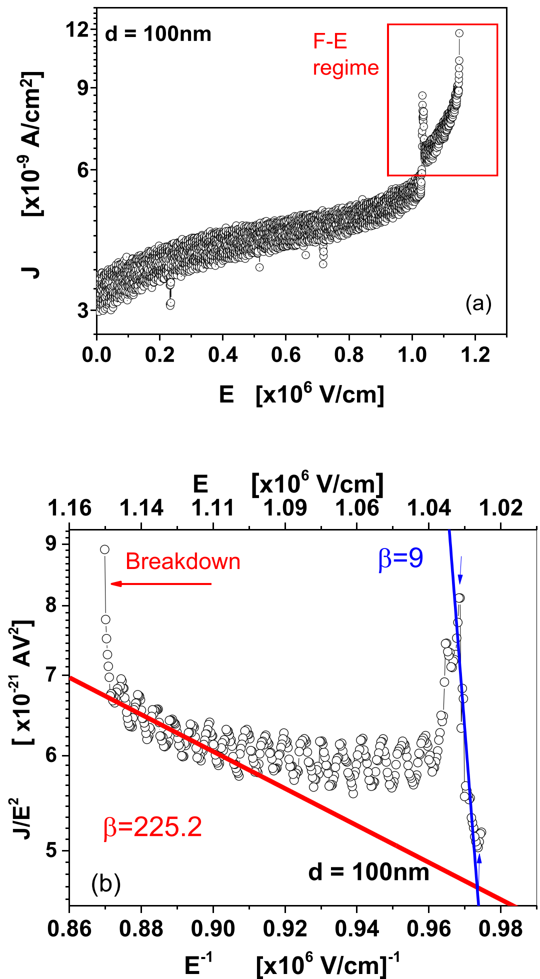

Fig. 4. (a) The I-V characteristic and (b) the Fowler-Nordheim plot of a device with 100 nm dielectric film.

4.3. The 200 nm dielectric film

The current-voltage (I-V) characteristic, up to breakdown threshold, of a MEMS capacitor with dielectric film of 200 nm is presented in Fig. 5a. In this case the field emission is clearly demonstrated and confirmed for electric fields larger than 10^6 V/cm through Fowler-Nordheim plot shown in Fig. 5b.

A comparison of electrical properties of the devices assessed in the present work reveals the presence of field emission through the measured current that flows through the MEMS capacitors gap. In all devices, the field emission is clearly confirmed through the Fowler-Nordheim plot. The devices with 100 nm dielectric film showed a minorly different behaviour since the field emission was observed at higher fields and close to breakdown. This behaviour has been attributed to reduced surface roughness.

5. Conclusions

The paper presents experimental evidence on field emission process in MEMS capacitors with rigid bridge and dielectric film of 50 nm, 100 nm and 200 nm. In these devices the dielectric film was deposited on the cathode, the bottom electrode. The field emission takes place through the dielectric film and occurs in all devices at electric fields larger than

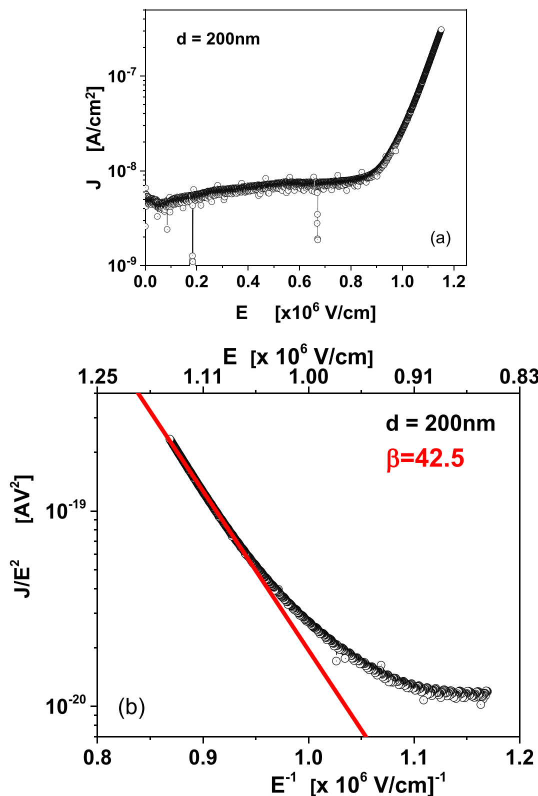

Fig. 5. (a) The I-V characteristic and (b) the Fowler-Nordheim plot revealing field emission mechanism.

10^6 V/cm. The intensity of field emission depends on the cathode surface roughness. According to these the field emission is expected to be present almost always in power MEMS applications since these devices will be designed to operate with higher DC voltages, which is the pull-in and therefore pull-out voltage and in addition to these, the presence of high RF voltage under hot or cold actuation.

CRediT authorship contribution statement

J. Theocharis: Investigation, Data curation, Software, Writing - Reviewing and editing,
S. Gardelis: Writing - Reviewing and editing, Supervision, Validation
G. Papaioannou: Conceptualization, Methodology, Writing - Reviewing and editing, Supervision, Funding acquisition, Validation.

Declaration of competing interest

The following authors have affiliations with organizations with direct or indirect financial interest in the subject matter discussed in the manuscript:

John Theocharis: Financed by the European Union and Greek national funds through the Operational Program Competitiveness, Entrepreneurship and Innovation, under the call RESEARCH – CREATE – INNOVATE (Project code: T1EDK-00329).

Data availability

The data that has been used is confidential.

Acknowledgements

The present work has been financed by the European Union and Greek national funds through the Operational Program Competitiveness, Entrepreneurship and Innovation, under the call RESEARCH – CREATE – INNOVATE (project code: T1EDK-00329).

References

[1] G. J. Papaioannou G. Wang D. Bessasm J. Papapolymerou , "Contactless dielectric charging mechanisms in RF-MEMS capacitive switches", 2006 European Microwave Integrated Circuits Conference (DOI:10.1109/EMICC.2006.282696).
[2] M. Koutsoureli, L. Michalas, P. Martins, E. Papandreou, A. Leuliet, S. Bansropun, A. Siaei, Properties of contactless and contacted charging in MEMS capacitive switches, Microelectron. Reliab. 53 (2013) 1655–1658, https://doi.org/10.1016/j.microrel.2013.07.057.
[3] G. Papaioannou, F. Giacomozzi, E. Papandreou, B. Margesin, Floating electrode microelectromechanical system capacitive switches: a different actuation mechanism, Appl. Phys. Lett. 99 (2011), 073501, https://doi.org/10.1063/1.3624830.
[4] L. Michalas, M. Koutsoureli, E. Papandreou, F. Giacomozzi, G. Papaioannou, Dielectric charging effects in floating electrode MEMS capacitive switches, Microelectron. Reliab. 55 (2015), https://doi.org/10.1016/j.microrel.2015.07.024, 1891-189.
[5] S. Mellé, D. De Conto, L. Mazenq, D. Dubuc, K. Grenier, L. Bary, O. Vendier, J. L. Muraro, J.L. Cazaux, R. Plana, Reliability modeling of capacitive RF MEMS, IEEE Trans. Microwave Theory Tech. 53 (2005) 3482–3488.
[6] X. Rottenberg, I.De Wolf, K.Bart K.J.C. Nauwelaers, W.r. De Raedt, H.A.C. Tilmans, Analytical model of the DC actuation of electrostatic MEMS devices with distributed dielectric charging and nonplanar electrodes, J. Microelectromech. Syst. 16 (2007) 1243–1253, https://doi.org/10.1109/JMEMS.2007.899334.
[7] R.W. Herfst P.G. Steeneken J. Schmitz A.J.G. Mank M. van Gils , "Kelvin probe study of laterally inhomogeneous dielectric charging and charge diffusion in RF MEMS capacitive switches", 2008 IEEE International Reliability Physics Symposium, (DOI:10.1109/RELPHY.2008.4558935).
[8] T.K.S. Wong, S.G. Ingram, J. Phys. D: Appl. Phys. 26, 979 (1993) "Observational of Fowler-Nordheim tunnelling at atmospheric pressure using Au/Ti lateral tunnel diodes, J. Phys. D: Appl. Phys. 26 (1993) 979, https://doi.org/10.1088/0022-3727/26/6/015.
[9] D.W. Branston, D. Stephani, Field emission from metal-coated silicon tips, IEEE Trans. Electron Devices 38 (1991) 2329–2333, https://doi.org/10.1109/16.88520.
[10] S.R. Pollack, Schottky field emission through insulating layer, J. Appl. Phys. 34 (1963) 877, https://doi.org/10.1063/1.1729554.
[11] K. Guang Yang, Ken Chin, R.B. Marcus, Electron field emission through a very thin oxide layer, IEEE Trans. Electron Devices 38 (1991) 2373–2376, https://doi.org/10.1109/16.88528.
[12] Myoung-Bok Lee, Sung-Ho Hahm, Jung-Hee Lee, Oon-Ho Song, Emission behavior of nm-thick Al2O3 film-based planar cold cathode for electronic cooling, Appl. Phys. Lett. 86 (2005), 123511, https://doi.org/10.1063/1.1894593.
[13] Yang Zhou Peng Zhang , "Field emission from dielectric coated metallic cathode surfaces: a theoretical study", 2021 22nd International Vacuum Electronics Conference (IVEC) DOI:10.1109/IVEC51707.2021.9722520.
[14] Yang Zhou, Peng Zhan, Theory of field emission from dielectric coated surfaces, Phys. Rev. Res. 2 (2020), 043439, https://doi.org/10.1103/PhysRevResearch.2.043439.
[15] A.Venkattraman Garg, A. Kovacs, A. Alexeenko, D. Peroulis, Direct measurements of field emission currents in e-static MEMS structures, in: IEEE MEMS Conf, 2011, pp. 412–415, https://doi.org/10.1109/MEMSYS.2011.5734449.